International Journal of Heat and Mass Transfer 197 (2022) 123330

Contents lists available at ScienceDirect

International Journal of Heat and Mass Transfer

journal homepage: www.elsevier.com/locate/hmt

Theoretical modeling of solid-liquid phase change in a phase change material protected by a multilayer Cartesian wall

Mohammad Parhizi[a], Long Zhou[b], Ankur Jain[c,*]

[a] UL Research Institutes, Houston, TX, USA
[b] School of Mechanical and Power Engineering, Polytechnic University, Jiaozuo, Henan, China
[c] Mechanical and Aerospace Engineering Department, University of Texas at Arlington, 500 W First St, Rm 211, Arlington, TX 76019, USA

ARTICLE INFO

Article history:
Received 16 March 2022
Revised 17 July 2022
Accepted 4 August 2022
Available online 26 August 2022

Keywords:
Phase change heat transfer
Multilayer wall
Moving boundary problems
Analytical modeling
Melting and solidification

ABSTRACT

Theoretical modeling of solid-liquid phase change processes is of much interest in energy storage and thermal management. While most theoretical phase change models assume that the phase change material (PCM) is in direct contact with the thermal source/sink, in most practical scenarios, the two are separated by a thick wall, which, in some cases, may comprise multiple heterogeneous layers. Accounting for thermal conduction through the multi-layer wall is important to ensure accuracy of the predicted phase change characteristics. This paper presents theoretical analysis of phase change in a system comprising a PCM and a multi-layer Cartesian wall using the eigenfunction expansion method and analysis of multi-layer thermal conduction. Thermal contact resistance between wall layers, and between the wall and PCM are accounted for. The predicted phase change front propagation is shown to agree well with past work for special case of a homogeneous wall, as well as with numerical simulations. Two distinct timescales in the solution, related to diffusion through the wall and phase change propagation in the PCM are identified. The impact of the imposed temperature, wall thermal diffusivity and thickness are presented in non-dimensional forms. Practical problems related to design of a PCM wall for energy storage are solved, showing two very different characteristics of stainless steel and polypropylene walls, as well as the impact of wall thickness on phase change propagation. The results presented here improve the fundamental understanding of phase change heat transfer processes, and are particularly relevant for relatively thick, thermally insulating walls over relatively short time periods, for which a resistance approximation for the wall is not accurate.

1. Introduction

Heat transfer during solid-liquid phase change has been used extensively for thermal management and energy storage by taking advantage of the large latent heat of phase change of materials. Prominent engineering processes and systems where phase change heat transfer plays a key role include thermal management of microelectronics [1], solar energy storage [2], additive manufacturing [3], food preservation [4], and metal casting [5]. The location of the solid-liquid interface in phase change heat transfer problems changes with time, resulting in significant mathematical complexity in solving such problems [6,7].

A considerable amount of research has been devoted for developing mathematical models for phase change heat transfer [8,9]. Determining the location of the phase change front as a function of time is usually of primary interest. However, unlike problems without phase change, exact solutions of phase change problems only exist for a limited number of simplified problems [6], such as one-dimensional, semi-infinite phase change problems with constant temperature boundary condition, commonly referred to as the Stefan problem, for which, the phase change interface location is proportional to $\sqrt{\alpha t}$ [10,11]. A wide variety of approximate analytical and numerical techniques have been developed for other, more complicated phase change problems. Quasi-stationary technique [6], integral method [12], perturbation method [13] and variable eigenvalue technique [14] are among the most commonly used approximate analytical methods. Such methods have been used to solve problems that present complications such as time-dependent boundary conditions [13,15], variable thermal properties [16,17], advection [18], steady-periodic regime [19,20], multiple phase change interfaces [21] and inverse heat transfer problems [22]. Several numerical techniques such as the enthalpy method [23], fixed and variable-grid methods [24], and the front-fixing method [25] have been developed and are used routinely to solve complicated phase change problems.

* Corresponding author.
E-mail address: jaina@uta.edu (A. Jain).

https://doi.org/10.1016/j.ijheatmasstransfer.2022.123330
0017-9310/

Nomenclature

C	heat capacity ($Jkg^{-1}K^{-1}$)
$\mathscr{L}$	latent heat of phase change (Jkg^{-1})
k	thermal conductivity ($Wm^{-1}K^{-1}$)
M	total number of layers
R	thermal contact resistance, (Km^2W^{-1})
$\bar{R}$	non-dimensional thermal contact resistance, $\bar{R}_m = \frac{k_L R_m}{x_M}$
Ste	Stefan number, $Ste = C_L(T_0 - T_f)/\mathcal{L}$
T	temperature (K)
x	spatial coordinate (m)
t	time (s)
α	thermal diffusivity (m^2s^{-1})
$\bar{\alpha}_m$	ratio of thermal diffusivities, $\bar{\alpha}_m = \frac{\alpha_m}{\alpha_L}$
$\bar{k}_m$	ratio of thermal conductivities, $\bar{k}_m = \frac{k_m}{k_L}$
τ	non-dimensional time, $\tau = \frac{\alpha_L t}{x_m^2}$
θ	non-dimensional temperature, $\theta_i = \frac{T_i - T_m}{T_{ref} - T_m}$, ($i$=L,1,2,3..M)
ξ	non-dimensional spatial coordinate, $\xi = \frac{x}{x_m}$
λ	non-dimensional eigenvalue
γ	non-dimensional interface location, $\gamma_m = \frac{x_m}{x_M}$

Subscripts

f	phase change temperature
in	initial temperature
L	liquid phase
LS	phase change front
m	layer number
0	imposed temperature

In most of the literature on phase change heat transfer, the phase change material (PCM) is assumed to be in direct contact with the heat source/sink. However, in practical scenarios, the PCM is usually enclosed in a thick-walled container (see, for example, Fig. 1(a)). For example, it is common for the PCM to be embedded within several cm thick concrete/brick wall [26] for building thermal management problems, or within an annular tube in flow problems [27]. Heat must first diffuse through the wall in order to cause phase change in the PCM. The wall itself may be single- or multi-layered. Depending on whether the goal is to maximize phase change of the PCM, or to insulate the PCM from the external source/sink, the thermal resistance/capacitance offered by the wall must be minimized or maximized, respectively. In some cases, the wall itself may be made of the same material as the PCM. A common example is in the freezing of a lake in winter, wherein any ice formed floats to the top and acts as an insulating wall to prevent further melting. An equivalent mass transfer problem of relevance is the growth of a passivation layer on a substrate that already has a finite passivation layer due to an initial reaction, or the combustion of a solid fuel particle that already has an ash layer surrounding the particle. In such cases, reactants must diffuse through a passive layer in order to reach the chemical reaction front. In each of these examples, it is important to develop analytical methods that accurately account for the effect of the wall, which can potentially be multi-layered, on the phase change process.

A number of papers have analyzed such phase change problems in the presence of a wall. The simplest approach is to represent each layer by a combination of resistance and capacitance (RC), which essentially neglects the temperature field within each layer [26]. In this work, the energy storage performance of a variety of PCM-embedded cementitious composites has been summarized. A lumped RC model has been used to solve a phase change problem in a multi-layer wall in a building [28]. Good agreement between RC modeling and computational fluid dynamics simulations was shown for specific cases. A similar model for concrete brick walls with embedded PCMs has also been proposed, based on which, the solar energy storage capability of a three-layered PCM wall in realistic conditions was predicted [29]. Such lumped models rely heavily on parameter estimation, and may lose accuracy when sensible energy storage within the non-PCM wall wall cannot be neglected, for example, when the wall is relatively thick. Numerical computational techniques have also been used to solve multi-layer heat transfer problems involving phase change. For example, an explicit finite difference method based on the enthalpy formulation has been used to solve a multi-layer pipeline problem with insulation and an intermediate PCM layer for long-distance subsea pipeline systems [27]. Numerical simulation has been used to investigate the performance of phase change materials in thick-walled triplex-tube and shell-and-tube energy storage units [30]. An implicit finite difference scheme has been used to solve a transient heat transfer problem involving a PCM and a multilayer wall [31]. Enthalpy-based numerical simulation has been used to solve problems involving multi-layer roofs and walls containing PCM [32,33]. In each of the papers cited above, the impact of mate-

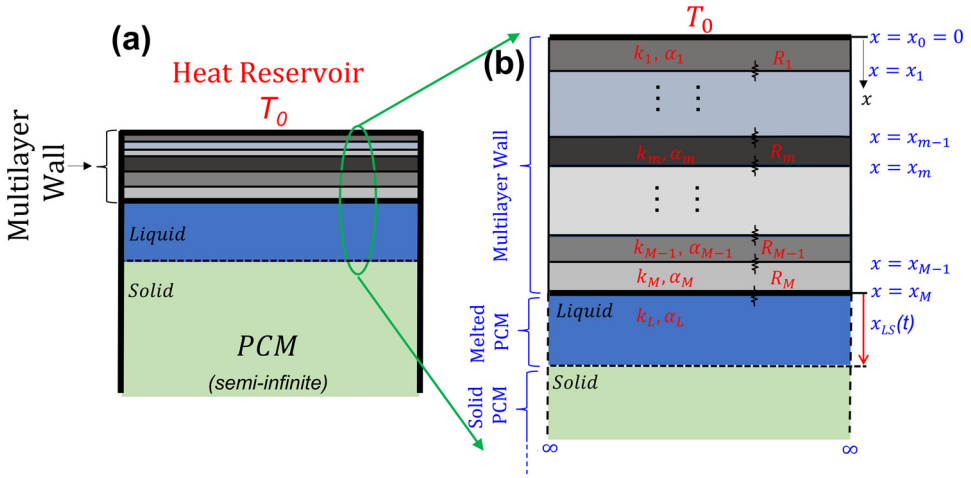

Fig. 1. Schematic geometry of the problem considered here: An M-layer non-melting wall is located above a semi-infinite phase change material. The composite body is heated up with a temperature boundary condition at the top. Heat diffusion through the M-layer wall and into the PCM results in melting and propagation of the phase change front. Distinct thermal properties of the layers, as well as thermal contact resistance between layers are considered.

rial properties and other problem parameters on phase change and temperature rise has been predicted using numerical simulations. While numerical models may be easy to implement, they are often computationally expensive and do not offer insights into the fundamental nature of the problem, such as the role of various non-dimensional numbers.

In contrast with the lumped models and numerical simulations described above, there is a relative lack of work on analytical modeling of phase change in a multi-layer body, such as PCM enclosed in a multilayered thick-walled container. The limited work available in this direction focuses on a single-layered wall [34,35]. The interaction of phase change process with diffusion in a multi-layer body makes this problem quite formidable. Such analytical models may be of much interest for developing a fundamental understanding of the problem and for parametric analysis. With suitable computational optimization, analytical solutions may compute faster than numerical simulations and without the need for proprietary software tools.

This paper derives an analytical solution for the problem of phase change of a material driven by a temperature boundary condition imposed across a multi-layer wall (Fig. 1). Heat transfer through the wall is accounted for by solving a multi-layer thermal conduction problem through the wall layers and the newly formed phase in the PCM. The resulting temperature distribution is used to determine the propagation of the phase change front as a function of time. Good agreement with past work for special cases and with numerical simulations is shown. The effect of various non-dimensional parameters such as Stefan number, as well as wall properties, such as thermal diffusivity and thickness is demonstrated. The analysis of two practical problems involving the melting of octadecane surrounded by a wall made of steel or polypropylene is solved. The next section defines the problem considered here, followed by presentation of the solution technique. Special cases are presented in Section 3. Key aspects of the results are also discussed in Section 4.

2. Problem definition

Fig. 1(a) shows a schematic of the problem under consideration. Fig. 1(b) presents further details of the geometry considered here, which comprises a semi-infinite PCM separated from a thermal source at constant temperature T_0 by an M-layered heterogeneous wall that does not undergo phase change. While the problem considered here involves melting of the PCM, solidification problems can be solved similarly. Thermal conductivity and diffusivity of the m^{th} layer are represented by k_m and α_m, respectively, for m=1,2..M. Similar properties of the liquid phase of the PCM are denoted by k_L and α_L, respectively. As shown in Fig. 1, the thickness of the m^{th} layer is given by (x_m-x_{m-1}). Total thickness of the wall is given by x_M. A thermal contact resistance R_m is assumed between the m^{th} and $(m+1)^{\text{th}}$ layers of the wall, for m=1,2..M-1. In addition, R_M refers to the thermal contact resistance between layer M of the wall and the phase change material. These contact resistances can be set to zero in order to model perfect thermal contact between adjacent materials. Latent heat of phase change of the PCM is denoted by $\mathcal{L}$. The initial temperature of the m^{th} layer is taken to be $T_{m,in}(x)$, (m=1,2…M), which is assumed to be larger than or equal to the melting temperature T_f, whereas the phase change material is assumed to be initially solid at the melting temperature T_f.

When measured from the wall-PCM interface, the initial thickness of the phase change front, x_{LS}, is zero, since the PCM is initially all solid. As heat diffuses through the multilayer wall and into the phase change material, the phase change front propagates into the semi-infinite PCM. A primary interest in such problems is to predict the phase change front, x_{LS} as a function of time, and to determine the impact of thermal properties and thicknesses of the non-melting wall layers on propagation of the phase change front.

Several standard assumptions are made for analysis of this problem. Heat transfer is assumed to be one-dimensional and driven purely by thermal conduction. Natural convection in the liquid PCM, as well as radiative heat transfer are neglected. All thermal properties are assumed to be independent of temperature. These assumptions are typically valid when the temperature difference is relatively small. Under these assumptions, the problem considered here may be mathematically described by the following governing energy equations:

$$\frac{\partial^2 T_m}{\partial x^2} = \frac{1}{\alpha_m}\frac{\partial T_m}{\partial t} \quad (x_{m-1} < x < x_m \ \ (m = 1, 2..M)) \tag{1}$$

$$\frac{\partial^2 T_L}{\partial x^2} = \frac{1}{\alpha_L}\frac{\partial T_L}{\partial t} \quad (x_M < x < x_M + x_{LS}(t)) \tag{2}$$

where T_m and T_L refer to the temperature fields in the m^{th} layer and in the liquid phase of phase change material, respectively. Since the PCM is initially solid at the melting temperature, and since the initial wall temperature is greater than T_f, therefore, no heat transfer occurs to/from the solid PCM. Associated boundary conditions for this problem are

$$T_1 = T_0 \quad (x = 0) \tag{3}$$

$$T_L = T_f \quad (x = x_M + x_{LS}(t)) \tag{4}$$

Eq. (3) arises from the constant temperature source imposed on top of the wall, whereas Eq. (4) arises from the phase change front always being at the melting temperature. In addition, the following interfacial conditions based on heat flux conservation and interfacial thermal resistance apply:

$$T_m = T_{m+1} - k_m R_m \frac{\partial T_m}{\partial x} \quad (x = x_m) \tag{5}$$

$$k_m \frac{\partial T_m}{\partial x} = k_{m+1}\frac{\partial T_{m+1}}{\partial x} \quad (x = x_m) \tag{6}$$

Eqs. (5) and (6) apply for m=1,2…M-1, and model thermal contact resistance and flux conservation at the interfaces within the wall. Similarly, at the wall-PCM interface, one may write

$$T_M = T_L - k_M R_M \frac{\partial T_M}{\partial x} \quad (x = x_M) \tag{7}$$

$$k_M \frac{\partial T_M}{\partial x} = k_L \frac{\partial T_L}{\partial x} (x = \ x_M) \tag{8}$$

The initial condition for this problem is given by known temperature distributions in each layer, i.e.,

$$T_m = T_{m,in}(x) \quad (t = 0) \tag{9}$$

for m=1,2..M. Finally, to complete the problem definition, energy conservation at the solid-liquid interface in the PCM is considered, as follows

$$-k_L\left(\frac{\partial T_L}{\partial x}\right)_{x=x_M+x_{LS}} = \ \rho_L \mathcal{L}\frac{dx_{LS}}{dt} \tag{10}$$

Note that temperature distribution in the semi-infinite solid does not appear in Eq. (10) since the solid is initially at the melting temperature and the wall initial temperature is greater than T_f, and therefore, no heat transfer to/from the solid occurs.

Note that setting M=1 in the problem definition above results in the problem of the PCM enclosed by a homogeneous, single-layered wall. Further, specific problems such as insulation of a

freezing lake by ice on the lake surface, or insulation of a PCM by previously-melted PCM [36] can be represented by setting the thermal properties of the wall and PCM to be the same.

Non-dimensionalization of the problem is carried out using the following variables: $\xi = \frac{x}{x_M}$, $\tau = \frac{\alpha_L t}{x_M^2}$, $\gamma_m = \frac{x_m}{x_M}$, $\theta_m = \frac{T_m - T_f}{T_0 - T_f}$, $\theta_L = \frac{T_L - T_f}{T_0 - T_f}$, $\bar{\alpha}_m = \alpha_m/\alpha_L$, $\bar{k}_m = k_m/k_L$, $\bar{R}_m = k_L R_m/x_M$ $(m$=1,2..$M)$, where the imposed temperature difference T_0-T_f and wall thickness x_M are used for non-dimensionalization. The following non-dimensional partial differential equations are obtained

$$\frac{\partial^2 \theta_m}{\partial \xi^2} = \frac{1}{\bar{\alpha}_m}\frac{\partial \theta_m}{\partial \tau} \ (\gamma_{m-1} < \xi < \gamma_m \ (m = 1, 2..M)) \tag{11}$$

$$\frac{\partial^2 \theta_L}{\partial \xi^2} = \frac{\partial \theta_L}{\partial \tau} \ (1 < \xi < 1 + \xi_{LS}(\tau)) \tag{12}$$

where $\xi_{LS} = \frac{x_{LS}}{x_M}$ is the non-dimensional location of the phase change front. Also, in Eq. (11), $\gamma_0 = 0$ based on the coordinate system shown in Fig. 1(b).

Associated boundary and interface conditions are

$$\theta_1 = 1 \ (\xi = 0) \tag{13}$$

$$\bar{k}_m \frac{\partial \theta_m}{\partial \xi} = \bar{k}_{m+1}\frac{\partial \theta_{m+1}}{\partial \xi} \ (\xi = \gamma_m) \tag{14}$$

$$\theta_m = \theta_{m+1} - \bar{k}_m \bar{R}_m \frac{\partial \theta_m}{\partial \xi} \ (\xi = \gamma_m) \tag{15}$$

$$\bar{k}_M \frac{\partial \theta_M}{\partial \xi} = \frac{\partial \theta_L}{\partial \xi} \ (\xi = 1) \tag{16}$$

$$\theta_M = \theta_L - \bar{k}_M \bar{R}_M \frac{\partial \theta_M}{\partial \xi} \ (\xi = 1) \tag{17}$$

$$\theta_L = 0 \ (\xi = 1 + \xi_{LS}(\tau)) \tag{18}$$

The non-dimensional initial conditions are

$$\theta_m = \theta_{m,in}(\xi) \ (\tau = 0) \tag{19}$$

$$\theta_L = 0 \ (\tau = 0) \tag{20}$$

where $\theta_{m,in} = \frac{T_{m,in} - T_f}{T_0 - T_f}$ is the initial non-dimensional temperature distribution within the m^{th} layer, and may be interpreted as the initial temperature in that layer relative to the melting temperature, non-dimensionalized by the temperature boundary condition, expressed similarly.

The non-dimensional equation for energy conservation at the interface is given by

$$\frac{1}{Ste}\frac{d\xi_{LS}}{d\tau} = -\frac{\partial \theta_L}{\partial \xi} \ (\xi = 1 + \xi_{LS}) \tag{21}$$

where $Ste = \frac{C_L(T_0 - T_f)}{\mathcal{L}}$ is the Stefan number. C_L refers to heat capacity of the liquid PCM.

The non-dimensional parameters appearing in this problem include Ste, which represents the imposed boundary condition, properties $\bar{\alpha}_m$ and $\bar{k}_m$, layer thicknesses γ_m, interface resistances $\bar{R}_m$ and initial temperatures $\theta_{m,in}$. The total wall thickness does not appear explicitly because it has been used as the lengthscale for non-dimensionalization.

The classical, no-wall Stefan problem admits a self-similarity based exact solution [6]. Due to the presence of a length scale in the present problem, however, it is unlikely that a self-similar solution is also applicable here. Instead, the method of eigenfunction expansion is used to seek an approximate analytical solution for this problem. Referring to Fig. 1, at any given time, the transient thermal conduction problem in the region above the phase change front (i.e., the multilayer wall and liquid phase of PCM) is solved. The resulting temperature distribution is differentiated at the location of the phase change front and inserted in the interfacial energy conservation, Eq. (21) to result in an ordinary differential equation that can be easily solved to determine the evolution of the phase change front. While this is an approximate solution, since the problem is reduced to one with constant ξ_{LS} at each time, nevertheless, solving the transient thermal conduction problem is expected to be an improvement over the quasi-stationary method [6], in which the transient term is completely ignored, and only the steady-state component of the solution is used.

The (M+1)-layer transient thermal conduction problem comprising the M-layer wall and liquid portion of the phase change material is a diffusion-driven multilayer problem with constant temperature boundary conditions at the two ends and interfacial contact resistance between adjacent layers. This problem can be solved using the theory of multilayer thermal conduction [37] that uses separation of variables technique and boundary/interfacial conditions to derive a single set of eigenvalues for all layers, followed by application of the initial condition and the principle of quasi-orthogonality to completely determine the temperature distribution in each layer. Since one of the boundary conditions is non-homogeneous, however, a substitution is first made to transfer the non-homogeneity from the boundary condition to the initial condition, as follows:

$$\theta_m(\xi, \tau) = s_m(\xi) + w_m(\xi, \tau) \ (m = 1, 2..M) \tag{22}$$

$$\theta_L(\xi, \tau) = s_L(\xi) + w_L(\xi, \tau) \tag{23}$$

Here, $s_m(\xi)$ and $s_L(\xi)$ are the steady-state components of the solution, governed by $s_m'' = 0$ and $s_L'' = 0$, respectively, along with the following boundary and interface conditions: $s_1(0) = 1$; $s_L(1 + \xi_{LS}) = 0$, $s_m(\gamma_m) = s_{m+1}(\gamma_m) - \bar{k}_m \bar{R}_m s_m'(\gamma_m)$, $\bar{k}_m s_m'(\gamma_m) = \bar{k}_{m+1} s_{m+1}'(\gamma_m)$, $s_M(1) = s_L(1) - \bar{k}_M \bar{R}_M s_M'(1)$, $\bar{k}_M s_M'(1) = \bar{k}_L s_L'(1)$. It can be shown that $s_m(\xi)$ and $s_L(\xi)$ are given by linear expressions as follows:

$$s_m(\xi) = A_m \xi + B_m \ (m = 1, 2, ..M) \tag{24}$$

$$s_L(\xi) = A_L \xi + B_L \tag{25}$$

where the coefficients A_m, B_m, A_L, B_L are given by

$$A_L = \left[-\frac{1}{\bar{k}_M} - \bar{R}_M - \xi_{LS} + \sum_{j=1}^{M-1} \left[\gamma_j \left(\frac{1}{\bar{k}_{j+1}} - \frac{1}{\bar{k}_j} \right) - \bar{R}_j \right] \right]^{-1} \tag{26}$$

$$B_L = -A_L(1 + \xi_{LS}) \tag{27}$$

$$A_m = \frac{A_L}{\bar{k}_m} \ (m = 1, 2, ..M) \tag{28}$$

$$B_m = A_L \left[-\frac{1}{\bar{k}_M} - \bar{R}_M - \xi_{LS} + \sum_{j=m}^{M-1} \left[\gamma_j \left(\frac{1}{\bar{k}_{j+1}} - \frac{1}{\bar{k}_j} \right) - \bar{R}_j \right] \right] \ (m = 1, 2, ..M) \tag{29}$$

On the other hand, the $w_m(\xi, \tau)$ and $w_L(\xi, \tau)$ problems represent diffusion in a (M+1)-layer body with homogeneous boundary

conditions given by the following

$$w_1 = 0 \ (\xi = 0) \tag{30}$$

$$\bar{k}_m \frac{\partial w_m}{\partial \xi} = \bar{k}_{m+1} \frac{\partial w_{m+1}}{\partial \xi} (\xi = \gamma_m) \ (m = 1, 2..M-1) \tag{31}$$

$$w_m = w_{m+1} - \bar{k}_m \bar{R}_m \frac{\partial w_m}{\partial \xi} \ (\xi = \gamma_m) \ (m = 1, 2..M-1) \tag{32}$$

$$\bar{k}_M \frac{\partial w_M}{\partial \xi} = \frac{\partial w_L}{\partial \xi} \ (\xi = 1) \tag{33}$$

$$w_M = w_L - \bar{k}_M \bar{R}_M \frac{\partial w_M}{\partial \xi} \ (\xi = 1) \tag{34}$$

$$w_L = 0 \ (\xi = 1 + \xi_{LS}(\tau)) \tag{35}$$

with non-homogeneous initial conditions given by

$$w_m = \theta_{m,in}(\xi) - s_m(\xi) \ (\tau = 0) \tag{36}$$

$$w_L = -s_L(\xi) \ (\tau = 0) \tag{37}$$

A solution for w_m and w_L may be obtained by writing a separable, eigenfunction-based series expansion of the type $w_m(\xi, \tau) = \sum_{n=1}^{\infty} f_{m,n}(\xi) g_n(\tau)$ and $w_L(\xi, \tau) = \sum_{n=1}^{\infty} f_{L,n}(\xi) g_n(\tau)$ as follows:

$$w_m(\xi, \tau) = \sum_{n=1}^{\infty} c_n \left[A_{m,n} \cos\left(\frac{\lambda_n}{\sqrt{\bar{\alpha}_m}}\xi\right) + B_{m,n} \sin\left(\frac{\lambda_n}{\sqrt{\bar{\alpha}_m}}\xi\right) \right] \exp\left(-\lambda_n^2 \tau\right) \tag{38}$$

$$w_L(\xi, \tau) = \sum_{n=1}^{\infty} c_n [A_{L,n} \cos(\lambda_n \xi) + B_{L,n} \sin(\lambda_n \xi)] \exp\left(-\lambda_n^2 \tau\right) \tag{39}$$

Here, the diffusivity term $\sqrt{\bar{\alpha}_m}$ is absorbed within the spatial terms instead of the transient term, in order to facilitate satisfying the interfacial conditions [37].

Eqs. (38) and (39), when substituted in the boundary and interface conditions given by Eqs. (30)–(35) result in

$$A_{1,n} = 0 \tag{40}$$

$$A_{m,n} \cos\left(\frac{\lambda_n \gamma_m}{\sqrt{\bar{\alpha}_m}}\right) + B_{m,n} \sin\left(\frac{\lambda_n \gamma_m}{\sqrt{\bar{\alpha}_m}}\right) = A_{m+1,n} \cos\left(\frac{\lambda_n \gamma_m}{\sqrt{\bar{\alpha}_{m+1}}}\right) + B_{m+1,n} \sin\left(\frac{\lambda_n \gamma_m}{\sqrt{\bar{\alpha}_{m+1}}}\right) - \bar{k}_m \bar{R}_m \frac{\lambda_n}{\sqrt{\bar{\alpha}_m}} \times \left[-A_{m,n} \sin\left(\frac{\lambda_n \gamma_m}{\sqrt{\bar{\alpha}_m}}\right) + B_{m,n} \cos\left(\frac{\lambda_n \gamma_m}{\sqrt{\bar{\alpha}_m}}\right) \right] \tag{41}$$

$$\frac{\bar{k}_m}{\sqrt{\bar{\alpha}_m}} \left[-A_{m,n} \sin\left(\frac{\lambda_n \gamma_m}{\sqrt{\bar{\alpha}_m}}\right) + B_{m,n} \cos\left(\frac{\lambda_n \gamma_m}{\sqrt{\bar{\alpha}_m}}\right) \right] = \frac{\bar{k}_{m+1}}{\sqrt{\bar{\alpha}_{m+1}}} \left[-A_{m+1,n} \sin\left(\frac{\lambda_n \gamma_m}{\sqrt{\bar{\alpha}_{m+1}}}\right) + B_{m+1,n} \cos\left(\frac{\lambda_n \gamma_m}{\sqrt{\bar{\alpha}_{m+1}}}\right) \right] \tag{42}$$

$$A_{M,n} \cos\left(\frac{\lambda_n}{\sqrt{\bar{\alpha}_M}}\right) + B_{M,n} \sin\left(\frac{\lambda_n}{\sqrt{\bar{\alpha}_M}}\right) = A_{L,n} \cos(\lambda_n) + B_{L,n} \sin(\lambda_n) - \bar{k}_M \bar{R}_M \frac{\lambda_n}{\sqrt{\bar{\alpha}_M}} \left[-A_{M,n} \sin\left(\frac{\lambda_n}{\sqrt{\bar{\alpha}_M}}\right) + B_{M,n} \cos\left(\frac{\lambda_n}{\sqrt{\bar{\alpha}_M}}\right) \right] \tag{43}$$

$$\frac{\bar{k}_M}{\sqrt{\bar{\alpha}_M}} \left[-A_{M,n} \sin\left(\frac{\lambda_n}{\sqrt{\bar{\alpha}_M}}\right) + B_{M,n} \cos\left(\frac{\lambda_n}{\sqrt{\bar{\alpha}_M}}\right) \right] = -A_{L,n} \sin(\lambda_n) + B_{L,n} \cos(\lambda_n) \tag{44}$$

$$A_{L,n} \cos(\lambda_n (1 + \xi_{LS})) + B_{L,n} \sin(\lambda_n (1 + \xi_{LS})) = 0 \tag{45}$$

Since Eqs. (40)–(45) are homogeneous, the determinant of these equations must be zero in order to ensure a non-trivial solution. This requirement results in an eigenequation for determining λ_n. As shown in Appendix A, the eigenequation is found to be

$$\frac{\bar{k}_M p_{M-1,n}(\gamma_{M-1}) \frac{\lambda_n}{\sqrt{\bar{\alpha}_M}} \cos\left(\frac{\lambda_n \gamma_{M-1}}{\sqrt{\bar{\alpha}_M}}\right) - \bar{k}_{M-1} \dot{p}_{M-1,n}(\gamma_{M-1}) \sin\left(\frac{\lambda_n \gamma_{M-1}}{\sqrt{\bar{\alpha}_M}}\right) - \bar{k}_{M-1} \bar{R}_{M-1} \dot{p}_{M-1,n}(\gamma_{M-1})}{\bar{k}_M p_{M-1,n}(\gamma_{M-1}) \frac{\lambda_n}{\sqrt{\bar{\alpha}_M}} \sin\left(\frac{\lambda_n \gamma_{M-1}}{\sqrt{\bar{\alpha}_M}}\right) + \bar{k}_{M-1} \dot{p}_{M-1,n}(\gamma_{M-1}) \cos\left(\frac{\lambda_n \gamma_{M-1}}{\sqrt{\bar{\alpha}_M}}\right)} + \frac{\tan\left(\frac{\lambda_n}{\sqrt{\bar{\alpha}_M}}\right) + \frac{\bar{k}_M}{\sqrt{\bar{\alpha}_M}} \tan(\lambda_n \xi_{LS}) - \frac{\bar{k}_M \bar{R}_M \lambda_n}{\sqrt{\bar{\alpha}_M}}}{1 - \frac{\bar{k}_M}{\sqrt{\bar{\alpha}_M}} \tan(\lambda_n \xi_{LS}) \tan\left(\frac{\lambda_n}{\sqrt{\bar{\alpha}_M}}\right) + \frac{\bar{k}_M \bar{R}_M \lambda_n}{\sqrt{\bar{\alpha}_M}} \tan\left(\frac{\lambda_n}{\sqrt{\bar{\alpha}_M}}\right)} = 0 \tag{46}$$

Where $p_{m,n}$ and $\psi_{m,n}$ are given by Eqs. (A.7)–(A.10) in Appendix A.

Once the eigenvalues are determined, the unknowns $A_{m,n}$, $B_{m,n}$, $A_{L,n}$ and $B_{L,n}$ may also be obtained. Due to the redundancy in Eqs. (40)–(45), one may assume $B_{1,n} = 1$ and determine the remaining coefficients from Eqs. (40) to (44). Explicit recursive expressions for these coefficients are derived in Appendix B. Finally, in order to determine c_n, Eqs. (38) and (39) are evaluated at $\tau = 0$, using the initial conditions given by Eqs. (36) and (37), followed by use of the principle of quasi-orthogonality of multilayer eigenfunctions. One may obtain

$$\theta_{m,in}(\xi) - s_m(\xi) = \sum_{n=1}^{\infty} c_n \left[A_{m,n} \cos\left(\frac{\lambda_n}{\sqrt{\bar{\alpha}_m}}\xi\right) + B_{m,n} \sin\left(\frac{\lambda_n}{\sqrt{\bar{\alpha}_m}}\xi\right) \right] \tag{47}$$

$$-s_L(\xi) = \sum_{n=1}^{\infty} c_n [A_{L,n} \cos(\lambda_n \xi) + B_{m,n} \sin(\lambda_n \xi)] \tag{48}$$

Finally, Eqs. (47) and (48) are multiplied by $\frac{\bar{k}_m}{\bar{\alpha}_m} [A_{m,n'} \cos(\frac{\lambda_{n'}}{\sqrt{\bar{\alpha}_m}}\xi) + B_{m,n'} \sin(\frac{\lambda_{n'}}{\sqrt{\bar{\alpha}_m}}\xi)]$ and $[A_{L,n'} \cos(\lambda_{n'}\xi) + B_{m,n'} \sin(\lambda_{n'}\xi)]$, respectively, followed by integration within the respective layers. The resulting equations are

added, which, based on quasi-orthogonality results in

$$c_n = \frac{1}{N_n}\left[\sum_{m=1}^{M}\left[\frac{\bar{k}_m}{\bar{\alpha}_m}\int_{\gamma_{m-1}}^{\gamma_m}[\theta_{m,0}(\xi)-s_m(\xi)]\left[A_{m,n}\cos\left(\frac{\lambda_n}{\sqrt{\bar{\alpha}_m}}\xi\right)+B_{m,n}\sin\left(\frac{\lambda_n}{\sqrt{\bar{\alpha}_m}}\xi\right)\right]d\xi\right]\right.$$
$$\left.+\int_{1}^{1+\xi_{LS}} -s_L(\xi)[A_{L,n}\cos(\lambda_n\xi)+B_{m,n}\sin(\lambda_n\xi)]d\xi\right] \quad (49)$$

where the norm N_n is given by

$$N_n = \sum_{m=1}^{M}\left[\frac{\bar{k}_m}{\bar{\alpha}_m}\int_{\gamma_{m-1}}^{\gamma_m}\left[A_{m,n}\cos\left(\frac{\lambda_n}{\sqrt{\bar{\alpha}_m}}\xi\right)+B_{m,n}\sin\left(\frac{\lambda_n}{\sqrt{\bar{\alpha}_m}}\xi\right)\right]^2 d\xi\right]$$
$$+\int_{1}^{1+\xi_{LS}}[A_{L,n}\cos(\lambda_n\xi)+B_{m,n}\sin(\lambda_n\xi)]^2 d\xi \quad (50)$$

This completes the formal solution for the general problem considered here, comprising an M-layer non-melting wall over a semi-infinite phase change material. Once the temperature distribution is determined, the derivative of the liquid temperature distribution at the liquid-solid interface, $\xi = 1+\xi_{LS}(\tau)$ can be inserted into Eq. (21) to result in the following ordinary differential equation for the phase change front location, $\xi_{LS}(\tau)$

$$\frac{d\xi_{LS}}{d\tau} = -Ste\left[A_L+\sum_{n=1}^{\infty}\lambda_n c_n[-A_{L,n}\sin(\lambda_n(1+\xi_{LS}))+B_{L,n}\cos(\lambda_n(1+\xi_{LS}))]\exp\left(-\lambda_n^2\tau\right)\right] \quad (51)$$

with $\xi_{LS}=0$ at $\tau=0$. While an analytical solution for Eq. (51) is unlikely to be obtainable, Eq. (51) provides an explicit expression for the derivative of ξ_{LS}, and therefore, can be easily integrated numerically to determine $\xi_{LS}(\tau)$.

3. Special cases

A special case of a single-layer wall shielding the phase change material from the temperature boundary condition is of particular interest for applications such as phase change material in a single-layered container. Solutions for the temperature distribution and phase change front propagation for this case may be derived by simply putting M=1 in results from Section 2. This results in

$$\theta_1(\xi,\tau) = 1-\frac{\xi}{1+\bar{k}_1\xi_{LS}+\bar{k}_1\bar{R}_1}+\sum_{n=1}^{\infty}c_n\sin\left(\frac{\lambda_n}{\sqrt{\bar{\alpha}_1}}\xi\right)\exp\left(-\lambda_n^2\tau\right) \quad (52)$$

$$\theta_L(\xi,\tau) = \frac{\bar{k}_1(1+\xi_{LS}-\xi)}{1+\bar{k}_1\xi_{LS}+\bar{k}_1\bar{R}_1}+\sum_{n=1}^{\infty}c_n\frac{\bar{k}_1}{\sqrt{\bar{\alpha}_1}}\frac{\sin(\lambda_n(\xi-(1+\xi_{LS})))}{\cos(\lambda_n\xi_{LS})}$$
$$\cos\left(\frac{\lambda_n}{\sqrt{\bar{\alpha}_1}}\right)\exp\left(-\lambda_n^2\tau\right) \quad (53)$$

where

$$c_n = \frac{1}{N_n}\left[\frac{\bar{k}_1}{\bar{\alpha}_1}\int_0^1\left[\theta_{1,0}(\xi)-1+\frac{\xi}{1+\bar{k}_1\xi_{LS}+\bar{k}_1\bar{R}_1}\right]\sin\left(\frac{\lambda_n}{\sqrt{\bar{\alpha}_1}}\xi\right)d\xi+\int_1^{1+\xi_{LS}}-\left(\frac{\bar{k}_1(1+\xi_{LS}-\xi)}{1+\bar{k}_1\xi_{LS}+\bar{k}_1\bar{R}_1}\right)\frac{\bar{k}_1}{\sqrt{\bar{\alpha}_1}}\frac{\sin(\lambda_n(\xi-(1+\xi_{LS})))}{\cos(\lambda_n\xi_{LS})}\cos\left(\frac{\lambda_n}{\sqrt{\bar{\alpha}_1}}\right)d\xi\right] \quad (54)$$

and the norm N_n is given by

$$N_n = \left[\frac{\bar{k}_1}{\bar{\alpha}_1}\int_0^1\sin^2\left(\frac{\lambda_n}{\sqrt{\bar{\alpha}_1}}\xi\right)d\xi+\int_1^{1+\xi_{LS}}\left[\frac{\bar{k}_1}{\sqrt{\bar{\alpha}_1}}\frac{\sin(\lambda_n(\xi-(1+\xi_{LS})))}{\cos(\lambda_n\xi_{LS})}\cos\left(\frac{\lambda_n}{\sqrt{\bar{\alpha}_1}}\right)\right]^2 d\xi\right] \quad (55)$$

and the eigenvalues are roots of $\frac{\sqrt{\bar{\alpha}_1}}{\bar{k}_1}\tan(\frac{\lambda_n}{\sqrt{\bar{\alpha}_1}})+\lambda_n\bar{R}_1+\tan(\lambda_n\xi_{LS})=0$. Note that this eigenequation can be obtained by either directly solving a two-layer problem, or by simply putting M=1 in the general eigenequation given by Eq. (46).

Subsequently, the differential equation for the phase change propagation front is given by

$$\frac{d\xi_{LS}}{d\tau} = -Ste\left[\frac{-\bar{k}_1}{1+\bar{k}_1\xi_{LS}+\bar{k}_1\bar{R}_1}+\sum_{n=1}^{\infty}\lambda_n c_n\frac{\bar{k}_1}{\sqrt{\bar{\alpha}_1}}\frac{\cos\left(\frac{\lambda_n}{\sqrt{\bar{\alpha}_1}}\right)}{\cos(\lambda_n\xi_{LS})}\exp\left(-\lambda_n^2\tau\right)\right] \quad (56)$$

with $\xi_{LS}=0$ at $\tau=0$.

A further special case of interest arises for a single-layer wall where the thermal properties of the wall and the PCM are the same, so that the wall represents a thickness of phase change material that is already in liquid form prior to t=0. This may represent scenarios where some phase change material has remained melted from a prior cycle of heat transfer into the phase change material. Another example for this scenario would be a finite thickness of pre-existing ice on top of a lake that shields liquid water in the lake from solidifying due to a cold ambient. In order to derive the results for this special case, one may insert $\bar{\alpha}_1=\bar{k}_1=1$ in Eqs. (52)–(56). This can be shown to result in a much simpler solution, in which, the temperature distribution in both pre-melted and newly-melted layers may be written as a combined expression

$$\theta_L(\xi,\tau) = 1-\frac{\xi}{1+\xi_{LS}}+\sum_{n=1}^{\infty}c_n\sin(\lambda_n\xi)\exp\left(-\lambda_n^2\tau\right) \quad (57)$$

where

$$c_n = \frac{2}{1+\xi_{LS}}\left[\int_0^1\left[\theta_{1,in}(\xi)-1+\frac{\xi}{1+\xi_{LS}}\right]\sin(\lambda_n\xi)d\xi\right.$$
$$\left.+\int_1^{1+\xi_{LS}}\left(-1+\frac{\xi}{1+\xi_{LS}}\right)\sin(\lambda_n\xi)d\xi\right] \quad (58)$$

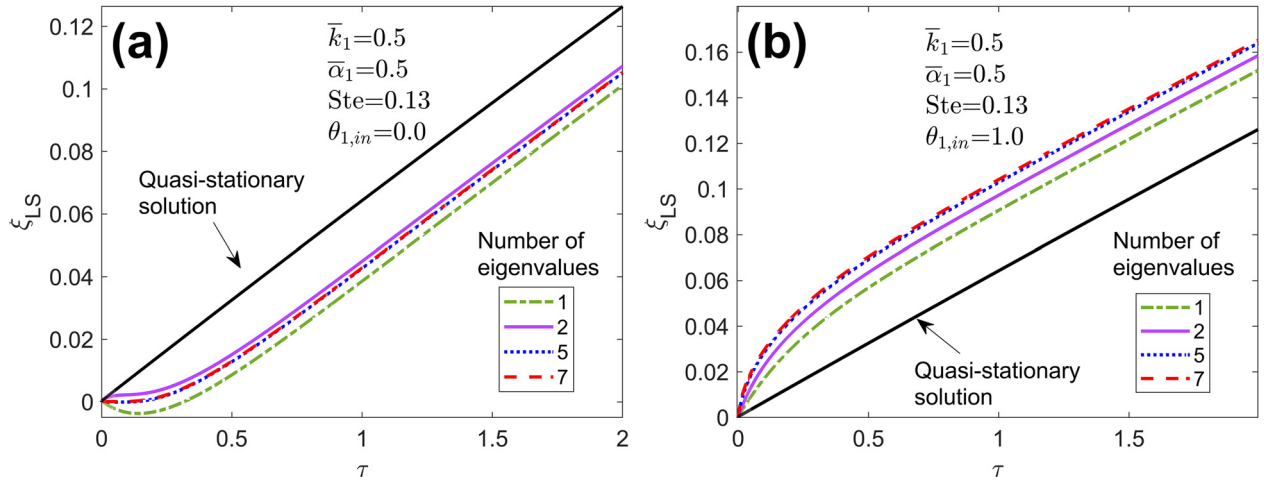

Fig. 2. Effect of number of eigenvalues considered in the solution: Phase change propagation front as a function of time for a single-layered wall on top of the PCM for (a) zero initial wall temperature, $\theta_{1,in} = 0.0$; (b) non-zero initial wall temperature, $\theta_{1,in} = 1.0$. In both cases, curves are plotted for different number of eigenvalues considered. Other parameters are $\bar{k}_1 = 0.5; \bar{\alpha}_1 = 0.5; Ste = 0.13; \bar{R}_1 = 0$.

and the differential equation for the phase change propagation front is given by

$$\frac{d\xi_{LS}}{d\tau} = -Ste\left[\frac{-1}{1+\xi_{LS}} + \sum_{n=1}^{\infty} \lambda_n c_n \cos(n\pi)\exp\left(-\lambda_n^2 \tau\right)\right] \tag{59}$$

where $\lambda_n = \frac{n\pi}{1+\xi_{LS}}$.

A final special case of interest is that of the wall being at zero temperature initially. For many problems, this is usually a reasonable approximation justified by the relatively large heat needed for phase change compared to sensible heating. Results for such a case may be derived by setting $\theta_{1,0} = 0$ in expressions above, both for the general M-layer wall (Section 2) and the two-layer wall discussed above, resulting in some simplification in expressions for c_n.

4. Results and discussion

4.1. Verification

Since the analytical solutions presented in Sections 2 and 3 are in the form of eigenvalue-based infinite series, it is important to determine the minimum number of eigenvalues needed to be considered to ensure acceptable accuracy. Note that eigenvalues for this problem must be re-computed at each time step as ξ_{LS} increases, which can be computationally expensive. Therefore, it is critical to determine the minimum number of eigenvalues needed for desired accuracy. This is particularly helpful for optimization of run-time computation of this problem that often needs to be carried out with limited computational resources.

For a representative problem with a single-layered wall on top of the PCM, Fig. 2 plots the predicted propagation of phase change front with time for different numbers of eigenvalues considered. Two cases with zero and non-zero initial temperature of the wall are presented in Fig. 2(a) and 2(b), respectively. These Figures also plot the zero eigenvalue case, which corresponds to the quasistationary solution that completely ignores transient conduction in the wall and liquid PCM. Both plots show that the eigenvalue-based series solution presented in this work differs significantly from the quasi-stationary solution, which does not correctly account for the role of the thick wall in the phase change process. These data also show that, in this case, around seven eigenvalues are sufficient for convergence of the predicted phase change propagation curve. Note that the shapes of converged plots for the zero and non-zero wall initial temperature differ from each other. In the zero initial temperature case, the phase change front propagates very slowly at first, due to time taken for heat to diffuse through the wall. On the other hand, when the wall itself is at a high initial temperature (in the case of Fig. 2(b), equal to the temperature of the imposed boundary condition), heat is readily transferred into the PCM from the wall, which is why, the phase change front rises rapidly at first, and then slows down.

Results from the present work are compared with a past paper for a special case of a single-layered wall with zero initial temperature. Hwang, et al. [34] presented analysis of this problem with zero initial temperature using the perturbation method. This method expresses the temperature distribution as a power series in terms of the Stefan number, based on which, the temperature distribution is determined through a term-by-term comparison. For comparison with this paper, the present model is computed with M=1 and $\theta_{1,in} = 0.0$. A comparison of phase change propagation as a function of time is presented in Fig. 3. Three cases of different values of thermal contact resistance and three cases of different values of Stefan number are presented in Fig. 3(a) and 3(b), respectively. There is excellent agreement between the perturbation method based results from Hwang, et al. [34] and the present work. As expected, the rate of phase change propagation increases with decreasing $\bar{R}_M$ or increasing Ste. Note that the results from Hwang, et al. are limited to a single-layered wall, with zero initial temperature, whereas the present work solves a much more general problem with an M-layered wall and non-zero initial temperature in each layer.

For additional verification of the present work, comparison of results with numerical simulations is also carried out. A finite-difference based numerical simulation technique is used for this purpose. A single layer wall in contact with PCM is considered here for validation purposes. The wall and PCM are discretized into a total of 2000 nodes. One node is considered at the wall-PCM interface to apply both heat flux and temperature continuity conditions. Heat transfer within the wall is purely conductive and is solved using the conventional implicit finite difference method. The heat transfer problem within the PCM, on the other hand, involves phase change and is solved using a variable timestep implicit finite difference method. The timestep in this problem is determined iteratively so that the phase change front moves only by one length interval during that time. Comparison between the two is presented in Fig. 4, where the phase change propagation front is plotted as a function of time for the one-phase problem with

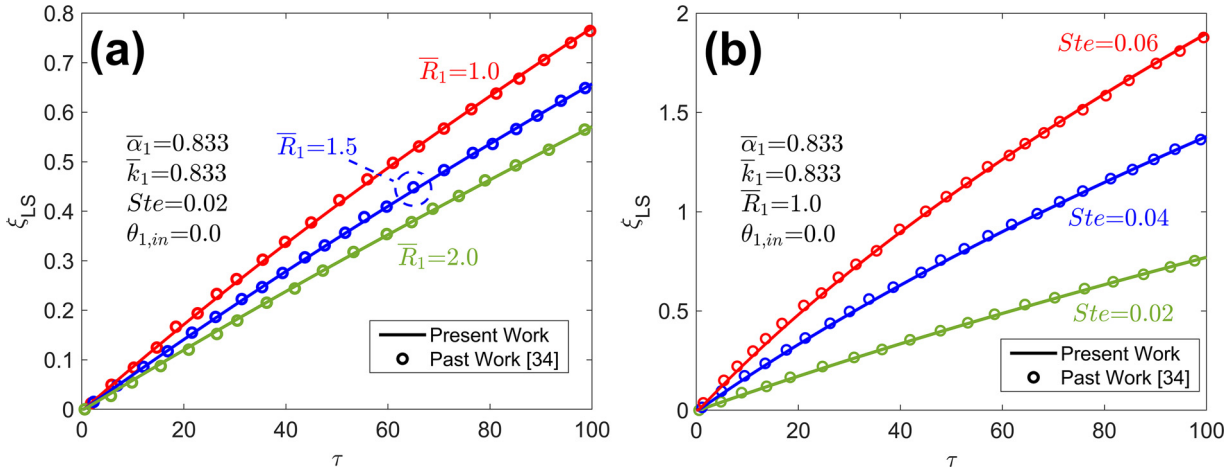

Fig. 3. Comparison with past work [34]: Phase change propagation front as a function of time for the special case of a single-layered wall on top of the PCM for (a) three different values of $\bar{R}_1$ at $Ste = 0.02$; (b) three different values of Ste at $\bar{R}_1 = 1.0$. In both cases, results from the present work (curves) are compared with past work based on perturbation method [34] (symbols). Other parameters are $\bar{k}_1 = 0.833; \bar{\alpha}_1 = 0.833;\ \theta_{1,in} = 0.0$.

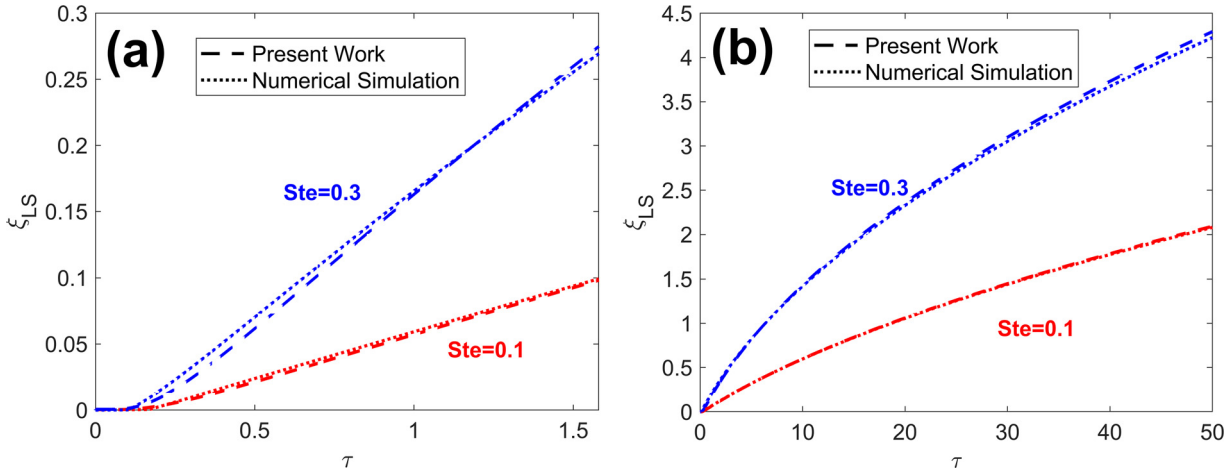

Fig. 4. Comparison with numerical simulations: Phase change propagation front as a function of time for a single-layered wall on top of the PCM at two different values of Ste over (a) short and (b) long time ranges. Other parameters are $\bar{k}_1 = 0.75; \bar{\alpha}_1 = 0.75; \theta_{1,in} = 0.0;\ \bar{R}_1 = 0$.

a homogeneous wall. Two sets of plots, for short and long time ranges are presented in Fig. 4(a) and 4(b), respectively. In each case, plots are presented for $Ste = 0.1$ and $Ste = 0.3$. These plots show excellent agreement between the analytical model and numerical simulations. As expected, ξ_{LS} increases with time, slowly at first due to diffusion through the non-melting layer (Fig. 4(a)), then more rapidly, and finally somewhat slower due to increasing thermal resistance of the melted layer (Fig. 4(b)). There is very good agreement between the analytical model and numerical simulation throughout both time scales for both values of Ste. The two distinct time scales involved in this process are investigated further in Section 4.2.

Fig. 5 shows results from a representative three-layer wall problem. Plots of the phase change front propagation as a function of time and temperature distributions at four different times are shown in Fig. 5(a) and 5(b), respectively. Problem parameters are $\bar{k}_1 = 0.833; \bar{\alpha}_1 = 0.833; \bar{k}_2 = 0.4; \bar{\alpha}_2 = 0.3; \bar{k}_3 = 0.6; \bar{\alpha}_3 = 0.8; \gamma_1 = 0.2; \gamma_2 = 0.8;\quad \theta_{1,in} = \theta_{2,in} = \theta_{3,in} = 0.0;\quad \bar{R}_1 = 1; \bar{R}_2 = 2;\quad \bar{R}_3 = 1$; Ste = 0.1. The phase change front starts slowly initially while heat diffuses through the multilayer wall, then rises rapidly. The temperature distributions exhibit discontinuity at interfaces between layers due to the non-zero thermal contact resistances. Propagation of the phase change front with time can also be seen in the temperature distribution plots.

4.2. Effect of Ste

The Stefan number is a key non-dimensional parameter for this problem that represents the magnitude of the imposed temperature boundary condition. In order to understand the effect of Ste on the temperature distribution and phase change front propagation process, the temperature distribution at $\tau = 20.52$ is plotted for different values of Ste in Fig. 6. A three-layered wall with zero initial temperature is considered. Problem parameters are $\bar{k}_1 = 0.3; \bar{\alpha}_1 = 0.4; \bar{k}_2 = 0.5; \bar{\alpha}_2 = 0.5; \bar{k}_3 = 0.6; \bar{\alpha}_3 = 0.6; \gamma_1 = 0.2; \gamma_2 = 0.8;\quad \theta_{1,in} = \theta_{2,in} = \theta_{3,in} = 0.0;\quad \bar{R}_1 = 0.5; \bar{R}_2 = 0; \bar{R}_3 = 0.5$. Fig. 6 shows the temperature distribution decaying from $\theta = 1$ at the hot boundary to $\theta = 0$ at the location of the phase change front. Discontinuities in the temperature distribution at the interfaces between layer 1 and layer 2, and layer 3 and liquid phase are seen, as a result of the non-zero thermal contact resistance values. In contrast, there is no discontinuity between layers 2 and 3 because $\bar{R}_2 = 0$. Fig. 6 also illustrates the impact of Ste – as Ste increases, the temperature distribution in each layer goes up due to greater flow of heat. In addition, the phase change front also propagates deeper into the PCM due to the small value of latent heat relative to sensible heat when Ste is large.

For further investigation of the impact of Ste, phase change propagation is plotted as a function of time for different values of

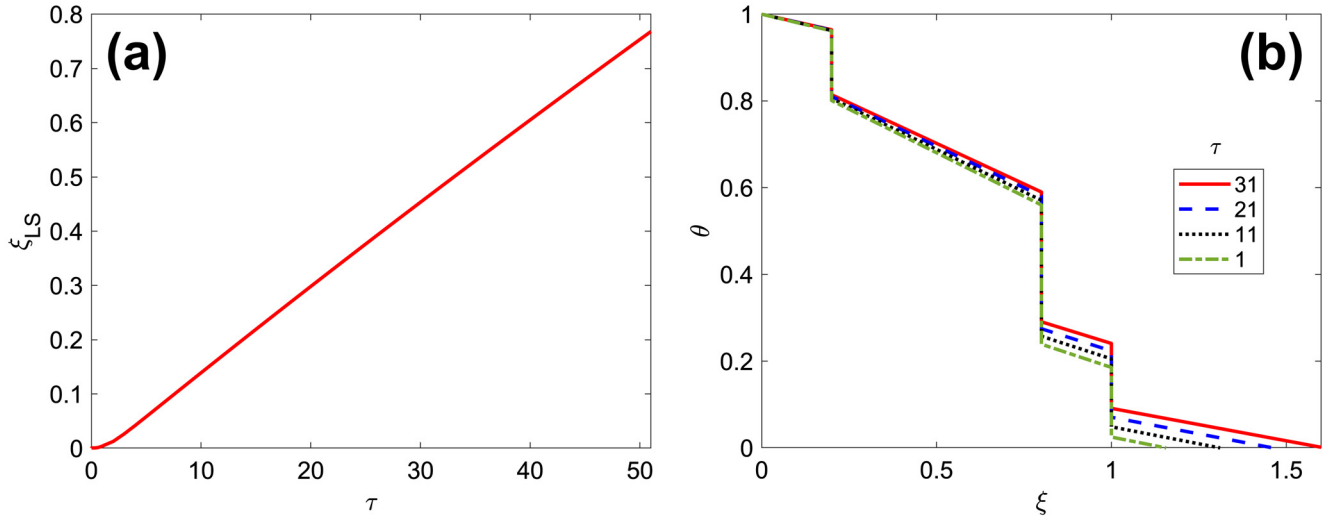

Fig. 5. Representative phase change front and temperature plots for a three-layered wall case: (a) phase change front as a function of time, and (b) temperature distributions at different times. Problem parameters are $\bar{k}_1 = 0.833$; $\tilde{\alpha}_1 = 0.833$; $\bar{k}_2 = 0.4$; $\tilde{\alpha}_2 = 0.3$; $\bar{k}_3 = 0.6$; $\tilde{\alpha}_3 = 0.8$; $\gamma_1 = 0.2$; $\gamma_2 = 0.8$; $\theta_{1,in} = \theta_{2,in} = \theta_{3,in} = 0.0$; $\bar{R}_1 = 1$; $\bar{R}_2 = 2$; $\bar{R}_3 = 1$; Ste $= 0.1$.

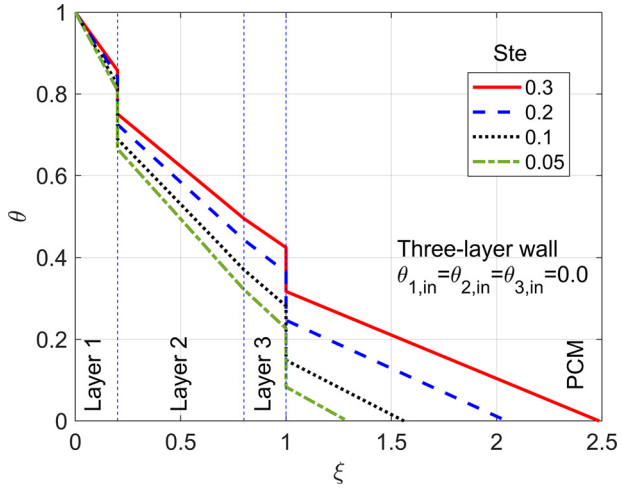

Fig. 6. Temperature distribution at $\tau = 20.52$ for a three-layered wall. Parameter values are $\bar{k}_1 = 0.3$; $\tilde{\alpha}_1 = 0.4$; $\bar{k}_2 = 0.5$; $\tilde{\alpha}_2 = 0.5$; $\bar{k}_3 = 0.6$; $\tilde{\alpha}_3 = 0.6$; $\gamma_1 = 0.2$; $\gamma_2 = 0.8$; $\theta_{1,in} = \theta_{2,in} = \theta_{3,in} = 0.0$; $\bar{R}_1 = 0.5$; $\bar{R}_2 = 0.0$; $\bar{R}_3 = 0.5$. Curves are plotted for different values of *Ste*.

Ste. The same problem parameters as Fig. 6 are considered. These plots are presented in Fig. 7(a) and 7(b) for short and long time ranges, respectively, in order to illustrate two key processes that govern phase change front propagation at different time scales. Fig. 7(a) shows the phase change front propagating very slowly initially, followed by a rapid rise. This is because the wall is initially at zero temperature, and therefore, heat needed for phase change must first diffuse from the imposed boundary through the cold wall and into the phase change material. Due to the finite diffusive time scale, phase change propagation is slow at first. Over a larger time scale, as shown in Fig. 7(b), the phase change propagation process proceeds rapidly at first, then slows down due to the increasing thermal resistance offered by the growing thickness of the melted layer. In both plots, the larger the value of *Ste*, the faster is the phase change propagation, as expected, since *Ste* represents the relative magnitude of the imposed boundary condition.

It is instructive to analyze similar results with a non-zero initial wall temperature. For the same three-layered wall as Fig. 7, except with $\theta_{1,in} = 1.0$, Fig. 8(a) and (b) plot phase change propagation over short and long time intervals, respectively. Unlike the zero initial wall temperature case (Fig. 7(a)), in this case, phase change propagation starts rapidly (Fig. 8(a)), because of thermal energy in the wall that can readily transfer into the PCM. As a result, over a short time period, at any given time, there is greater phase change propagation in this case compared to zero initial wall temperature. Over a longer time period, however, as thermal diffusion from the boundary condition begins to dominate, the difference between the two cases (Figs. 7(b) and 8(b)) diminishes, particularly for large *Ste*. This is because at large *Ste*, the impact of the boundary condition dominates over that of the initial wall temperature. When *Ste* is small, the effect of the initial wall temperature persists over a longer time, resulting in greater melting.

4.3. Effect of initial temperature

In order to further understand the effect of the wall initial temperature, phase change propagation curves are plotted for three different values of $\theta_{1,in}$. Results are presented for a single-layered wall for both short and large time periods in Fig. 9(a) and 9(b), respectively. Phase change propagation begins slowly for the zero wall initial temperature case due to the time taken from heat from the imposed boundary condition to diffuse through the wall. On the other hand, when the wall itself has a non-zero initial temperature, the heat from the wall diffuses readily into the PCM, resulting in rapid initial phase change propagation. After some time, each curve rises at roughly the same rate. As expected, the larger the initial temperature, the higher is the corresponding phase change propagation curve. However, as shown in Fig. 9(b), the impact of the initial temperature diminishes over a longer time period, and the three curves nearly coincide. This is because, unless $\theta_{1,in}$ is unrealistically large, the additional phase change due to initial thermal energy of the wall is quite small compared to phase change driven by the external boundary condition. It can be shown that the non-dimensional thickness of PCM that melts due to the initial thermal energy in the wall is of the order of $Ste \cdot \theta_{1,in}$. Based on the parameters used here, the offset between zero and non-zero initial temperature curves in Fig. 9(a) is consistent with this estimate. Note that over a longer time period, as the thickness of the newly melted liquid grows, there is increased resistance to heat flow into the phase change front, resulting in a slowdown of the melting process. This is clearly seen in Fig. 9(b).

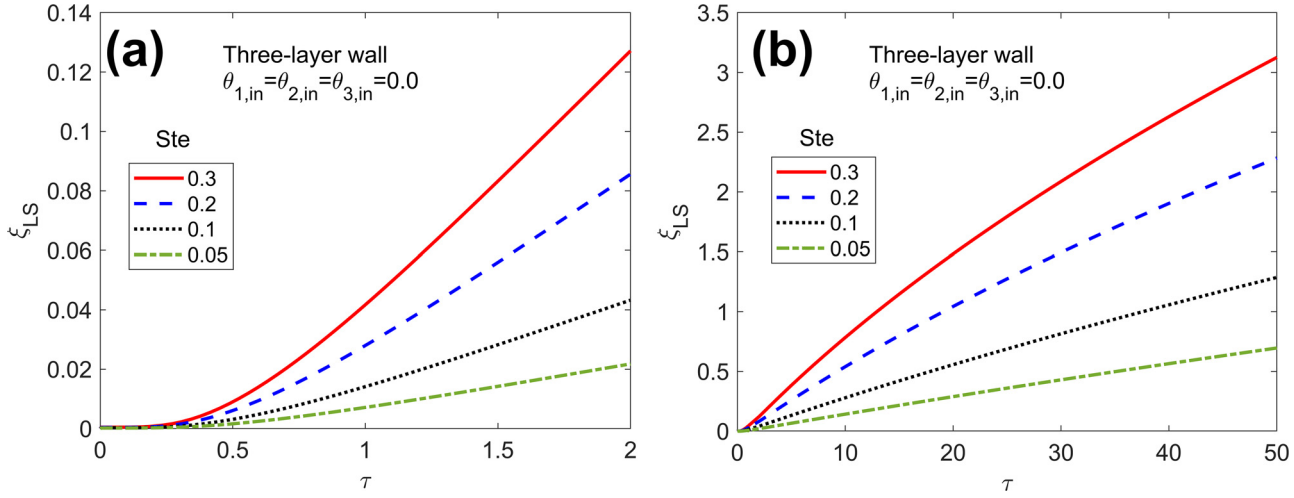

Fig. 7. Effect of Stefan number for zero initial temperature of a three-layer wall: Phase change propagation front as a function of time for different values of *Ste*. (a) and (b) present plots over short and long time ranges, respectively. Problem parameters are the same as Fig. 5.

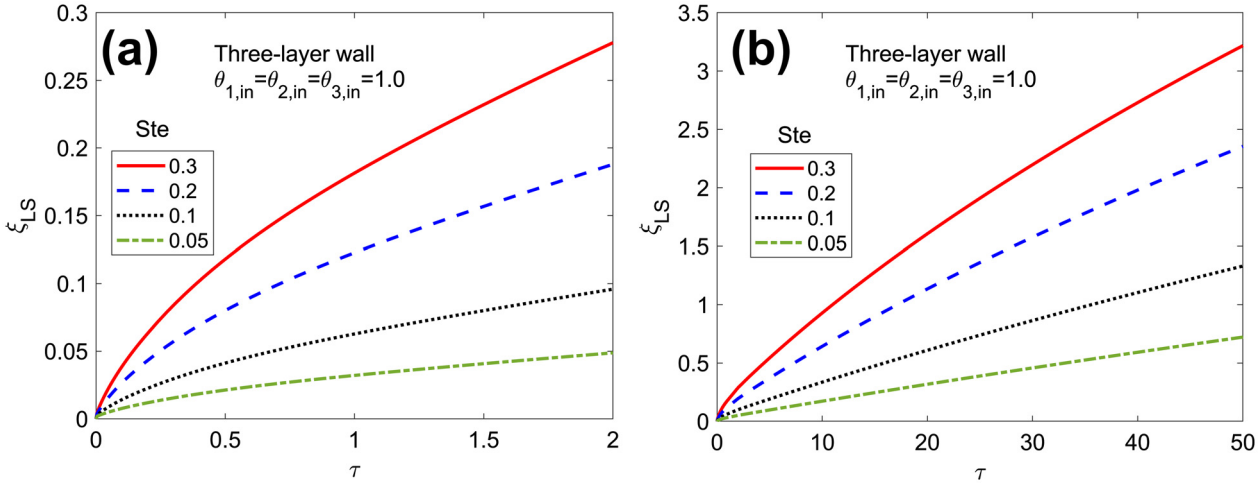

Fig. 8. Effect of Stefan number for non-zero initial temperature of a three-layer wall: Phase change propagation front as a function of time for different values of *Ste*. (a) and (b) present plots over short and long time ranges, respectively. Problem parameters are $\bar{k}_1 = 0.3; \bar{\alpha}_1 = 0.4; \bar{k}_2 = 0.5; \bar{\alpha}_2 = 0.5; \bar{k}_3 = 0.6; \bar{\alpha}_3 = 0.6; \gamma_1 = 0.2; \gamma_2 = 0.8;\ \theta_{1,in} = \theta_{2,in} = \theta_{3,in} = 1.0;\ \bar{R}_1 = 0.5; \bar{R}_2 = 0.0; \bar{R}_3 = 0.5$.

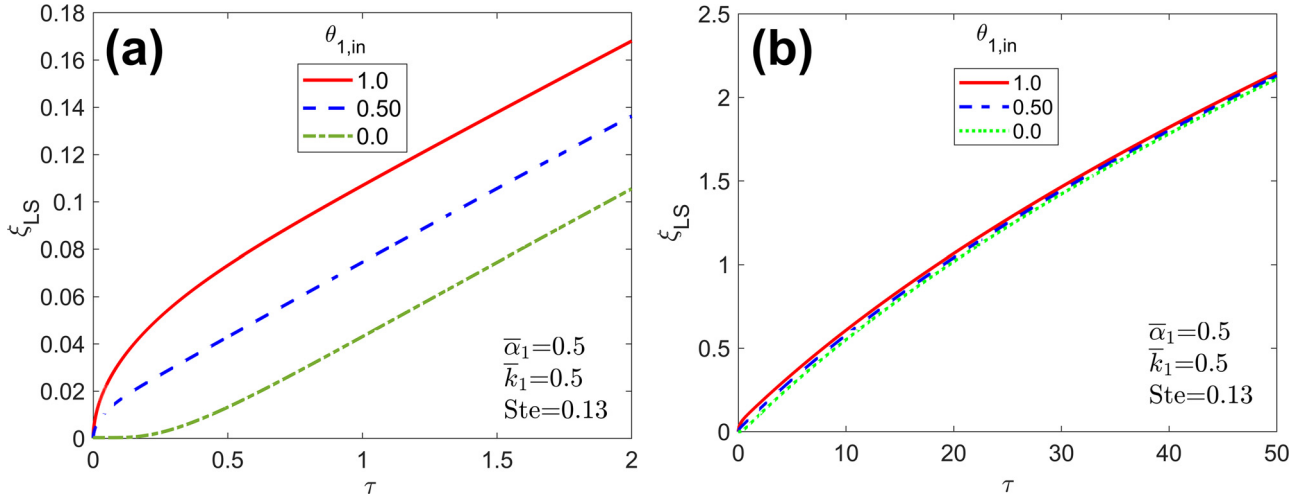

Fig. 9. Effect of the initial temperature distribution in the wall: Phase change propagation front as a function of time for a single-layered wall for different values of $\theta_{1,in}$. (a) and (b) present plots over short and long time ranges, respectively. Other parameters are $\bar{k}_1 = 0.5; \bar{\alpha}_1 = 0.5; Ste = 0.13;\ \bar{R}_1 = 0$.

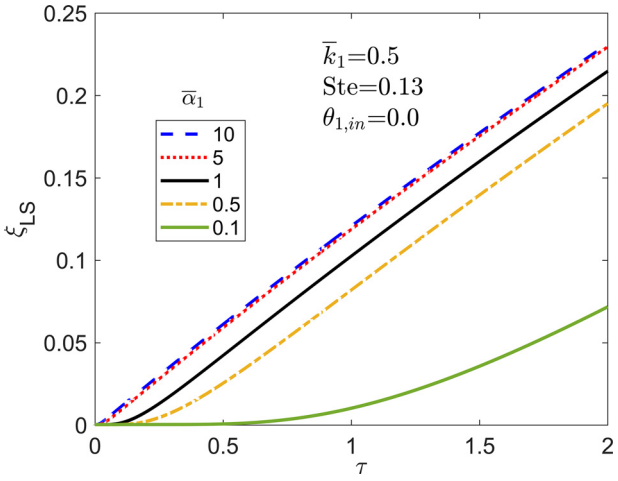

Fig. 10. Effect of thermal diffusivity of the wall: Phase change propagation front as a function of time for a single-layered wall for different values of $\bar{\alpha}_1$, ranging from a poorly diffusive wall to a highly diffusive wall. Other parameters are $\bar{k}_1 = 0.5$; $Ste = 0.13$; $\theta_{1,in} = 0$; $\bar{R}_1 = 0$.

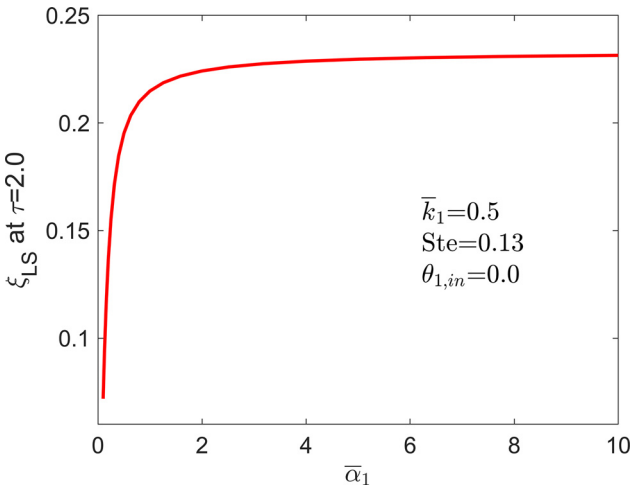

Fig. 11. Effect of thermal diffusivity of the wall: Phase change propagation front at $\tau = 2$ for a single-layered wall as a function of $\bar{\alpha}_1$, ranging from a poorly diffusive wall to a highly diffusive wall. Other parameters are $\bar{k}_1 = 0.5$; $Ste = 0.13$; $\theta_{1,in} = 0$; $\bar{R}_1 = 0$.

4.4. Effect of wall thermal properties

The key thermal property of the wall that governs the phase change propagation is its thermal diffusivity, $\bar{\alpha}_1$. Note that $\bar{\alpha}_1 > 1$ represents a wall that is more diffusive than the PCM, for example, a metal wall enclosing a typical PCM. On the other hand, $\bar{\alpha}_1 < 1$ represents a case where the wall has lower diffusivity than the PCM, which may be needed when the goal is to thermally insulate the PCM and prevent it from melting/solidification. This may occur, for example, in a solar thermal energy storage system, where the PCM after melting must be stored in heavily insulated conditions in order to preserve its thermal energy for later use.

Phase change front location is calculated as a function of time for a number of values of $\bar{\alpha}_1$. Results are plotted in Fig. 10. A small value of $\bar{\alpha}_1$ results in slow start to the phase change propagation process, which is because heat takes longer to diffuse through the wall when $\bar{\alpha}_1$ is small. Even with $\bar{\alpha}_1 = 1$, there is an initial time period during which, the rate of phase change propagation is very small. Interestingly, Fig. 10 shows a saturation effect for very large values of $\bar{\alpha}_1$. For example, curves corresponding to $\bar{\alpha}_1 = 5$ and $\bar{\alpha}_1 = 10$ are nearly identical. This is primarily because once the wall thermal diffusivity is large enough, it is no longer the rate-limiting step, and, therefore, further improving the wall thermal diffusivity has only a negligible effect on phase change propagation. In order to investigate this further, the location of the phase change front at $\tau = 2$ is plotted as a function of $\bar{\alpha}_1$ in Fig. 11. This plot clearly shows the saturation effect, wherein there is negligible improvement in the phase change process beyond a value of around $\bar{\alpha}_1 = 2$.

4.5. An alternate non-dimensionalization of the spatial variable

Classical phase change problems, such as the one-dimensional, no-wall Stefan problem do not have a length scale, due to which, non-dimensionalization is usually carried out using an arbitrary reference length. In the present problem, the wall thickness is a naturally available length scale, and therefore, is used in non-dimensionalization of the problem. As a result of this, however, the wall thickness remains embedded within the non-dimensional parameters, and it is difficult to examine the impact of the wall thickness of the phase change process.

As an alternate approach to solving this problem, non-dimensionalization is carried out using an arbitrary length L_{ref}, which preserves the wall thickness as an explicit non-dimensional parameter in the problem. This is illustrated below for a single-layer wall problem with perfect thermal contact. The following non-dimensionalization is used: $\xi = \frac{x}{L_{ref}}$, $\tau = \frac{\alpha_L t}{L_{ref}^2}$, $\theta_1 = \frac{T_1 - T_f}{T_{ref} - T_f}$, $\theta_L = \frac{T_L - T_f}{T_{ref} - T_f}$, $\bar{\alpha}_1 = \alpha_1/\alpha_L$, $\bar{k}_1 = k_1/k_L$, $\xi_1 = x_1/L_{ref}$. Here, ξ_1 is the non-dimensional wall thickness that did not appear in the treatment in Sections 2 and 3. The resulting problem is quite similar to the problem solved in Section 3. The temperature distribution in the wall and in the melted PCM, $\theta_1(\xi, \tau)$ and $\theta_L(\xi, \tau)$ can be shown to be

$$\theta_1(\xi,\tau) = 1 - \frac{\xi}{\xi_1\left[1 + \bar{k}_1\xi_{LS}/\xi_1\right]} + \sum_{n=1}^{\infty} c_n \sin\left(\frac{\lambda_n}{\sqrt{\bar{\alpha}_1}}\xi\right)\exp\left(-\lambda_n^2\tau\right) \tag{60}$$

$$\theta_L(\xi,\tau) = \frac{\bar{k}_1(\xi_1 + \xi_{LS} - \xi)}{\xi_1\left[1 + \bar{k}_1\xi_{LS}/\xi_1\right]} + \sum_{n=1}^{\infty} c_n \frac{\sin\left(\lambda_n(\xi_1 + \xi_{LS} - \xi)\right)}{\sin\left(\lambda_n\xi_{LS}\right)} \sin\left(\frac{\lambda_n\xi_1}{\sqrt{\bar{\alpha}_1}}\right)\exp\left(-\lambda_n^2\tau\right) \tag{61}$$

where

$$c_n = \frac{1}{N_n}\left[\frac{\bar{k}_1}{\bar{\alpha}_1}\int_0^{\xi_1}\left[\theta_{1,0}(\xi) - \left(1 - \frac{\xi}{\xi_1\left[1 + \bar{k}_1\xi_{LS}/\xi_1\right]}\right)\right]\sin\left(\frac{\lambda_n}{\sqrt{\bar{\alpha}_1}}\xi\right)d\xi + \int_{\xi_1}^{\xi_1+\xi_{LS}} -\frac{\bar{k}_1(\xi_1 + \xi_{LS} - \xi)}{\xi_1\left[1 + \bar{k}_1\xi_{LS}/\xi_1\right]}\frac{\sin\left(\lambda_n(\xi_1 + \xi_{LS} - \xi)\right)}{\sin\left(\lambda_n\xi_{LS}\right)}\sin\left(\frac{\lambda_n\xi_1}{\sqrt{\bar{\alpha}_1}}\right)d\xi\right] \tag{62}$$

and the norm N_n is given by

$$N_n = \left[\frac{\bar{k}_1}{\bar{\alpha}_1}\int_0^{\xi_1}\sin^2\left(\frac{\lambda_n}{\sqrt{\bar{\alpha}_1}}\xi\right)d\xi + \int_{\xi_1}^{\xi_1+\xi_{LS}}\frac{\sin^2\left(\lambda_n(\xi_1+\xi_{LS}-\xi)\right)}{\sin^2\left(\lambda_n\xi_{LS}\right)}\sin^2\left(\frac{\lambda_n\xi_1}{\sqrt{\bar{\alpha}_1}}\right)d\xi\right] \tag{63}$$

and the eigenvalues are roots of $\frac{\sqrt{\bar{\alpha}_1}}{\bar{k}_1}\tan\left(\frac{\lambda_n\xi_1}{\sqrt{\bar{\alpha}_1}}\right) + \tan\left(\lambda_n\xi_{LS}\right) = 0$.

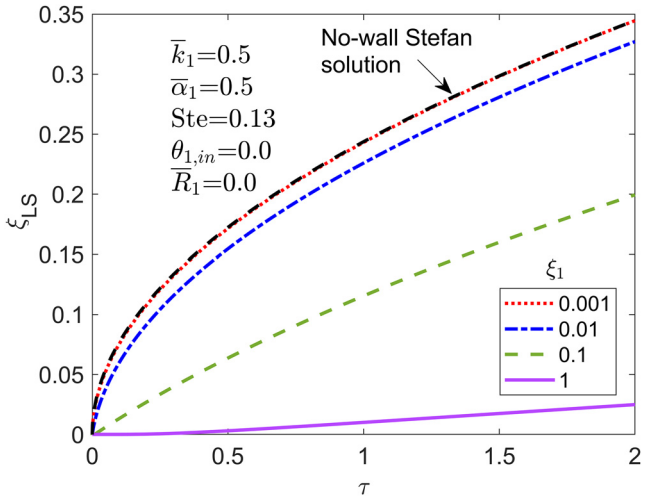

Fig. 12. Effect of wall thickness: Phase change propagation front as a function of time for a single-layered wall for different values of the wall thickness. Other parameters are $\bar{k}_1 = 0.5; \bar{\alpha}_1 = 0.5;\ \ Ste = 0.13; \theta_{1,in} = 0;\ \ \bar{R}_1 = 0$. Note that non-dimensionalization in this Figure follows the scheme discussed in Section 4.5, with $L_{ref} = 1\ m$.

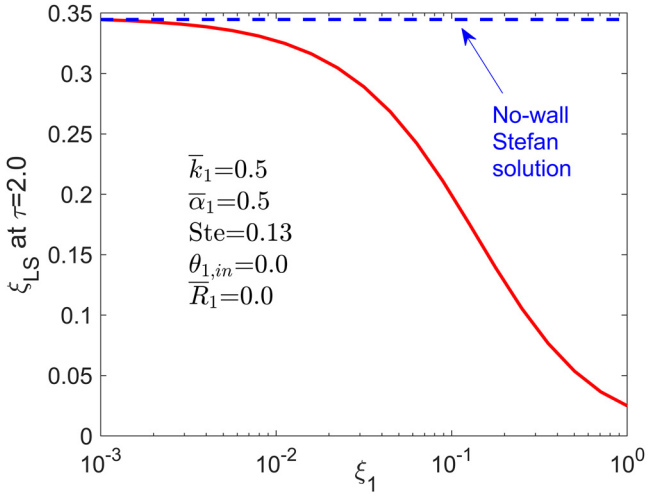

Fig. 13. Effect of wall thickness: Phase change propagation front as a function of time for a single-layered wall for different values of the wall thickness. Other parameters are $\bar{k}_1 = 0.5; \bar{\alpha}_1 = 0.5;\ \ Ste = 0.13; \theta_{1,in} = 0;\ \ \bar{R}_1 = 0$. Note that non-dimensionalization in this Figure follows the scheme discussed in Section 4.5, with $L_{ref} = 1\ m$.

Subsequently, the ODE for the phase change propagation front is given by

$$\frac{d\xi_{LS}}{d\tau} = -Ste\left[\frac{-\bar{k}_1}{\xi_1\left[1+\bar{k}_1\xi_{LS}/\xi_1\right]} - \sum_{n=1}^{\infty}\lambda_n c_n \frac{\sin\left(\frac{\lambda_n\xi_1}{\sqrt{\bar{\alpha}_1}}\right)}{\sin\left(\lambda_n\xi_{LS}\right)}\exp\left(-\lambda_n^2\tau\right)\right] \tag{64}$$

Due to the explicit appearance of the non-dimensional wall thickness, ξ_1 in the solution, it is easier to understand the impact of wall thickness on phase change process through this alternate non-dimensionalization.

Fig. 12 plots the phase change propagation as a function of time for a number of different wall thicknesses, ξ_1. Results indicate that the thicker the wall, the slower is the phase change propagation process. This is an expected result, because the time taken for heat diffusion through the wall is longer for a thicker wall. Fig. 12 shows extremely slow phase change for a very thick wall, $\xi_1 = 1$. On the other hand, as the wall thickness becomes smaller and smaller, Fig. 12 shows that the phase change propagation curve is faster and faster, and approaches the solution for the classical Stefan problem with no wall, for which, the solution is $\xi_{LS} = 2\lambda\sqrt{\tau}$, where λ is the root of $x\text{erf}(x)\exp(x^2) = Ste/\sqrt{\pi}$. A saturation effect similar to the one seen for wall thermal diffusivity in Fig. 11 is also seen for wall thickness in Fig. 12. A plot of ξ_{LS} at $\tau = 2.0$ as a function of wall thickness ξ_1 in Fig. 13 clearly shows that the solution approaches the result from the standard no-wall Stefan solution when ξ_1 is around 0.002 or lower.

4.6. Solution of a practical problem

All of the plots presented so far are in non-dimensional form in order to help understand the fundamentals of this problem. The analytical model is next used to solve two representative practical problems in dimensional form. First, the impact of the wall material on phase change propagation in octadecane is analyzed. A 30°C temperature boundary condition, relative to melting temperature is assumed. The wall and PCM are both assumed to be initially at the melting temperature. For a 1 cm thick wall, phase change propagation as a function of time is plotted for two different wall materials – stainless steel 304 and polypropylene. Wall thermal properties

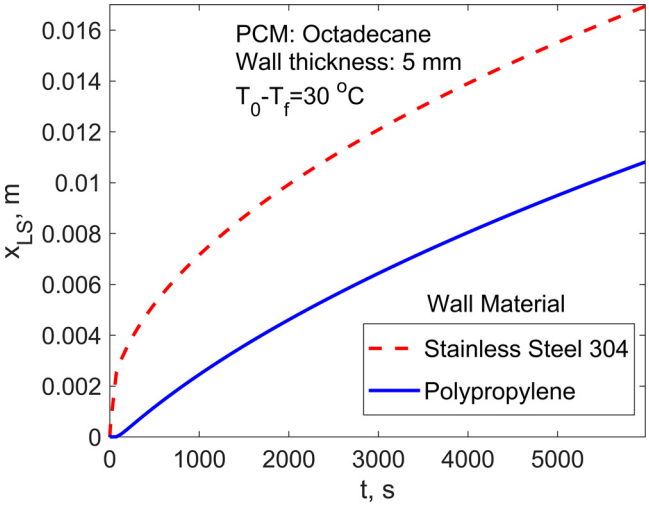

Fig. 14. Analysis of a practical problem: Phase change propagation front as a function of time for a single-layered 1 cm thick wall with octadecane phase change material and 30 K temperature boundary condition relative to melting temperature. Both wall and PCM are assumed to be at melting temperature initially. Plots are presented in dimensional form for two different wall materials.

are taken from a past paper [38] and from manufacturer specifications [39], respectively. PCM thermal properties are also taken from past work [40,41]. The resulting plot is presented in Fig. 14, which shows, as expected, a greater rate of phase change propagation for stainless steel due to greater thermal conductivity and thermal diffusivity than polypropylene. A high diffusivity material such as steel is preferable over polypropylene for the wall when the goal is to facilitate phase change in the PCM.

For a similar problem with octadecane as the PCM and polypropylene as the wall material, the impact of wall thickness is analyzed in Fig. 15. Phase change propagation as a function of time is plotted for a number of wall thicknesses. Similar to Fig. 14, a 30°C temperature boundary condition, relative to melting temperature is assumed, and both wall and PCM are assumed to be at melting temperature initially. Fig. 15 shows, as expected, that the phase change front propagates faster and faster as the wall thickness reduces. In each curve, there is a short initial period, in which, the melting process is very slow due to the time taken for ther-

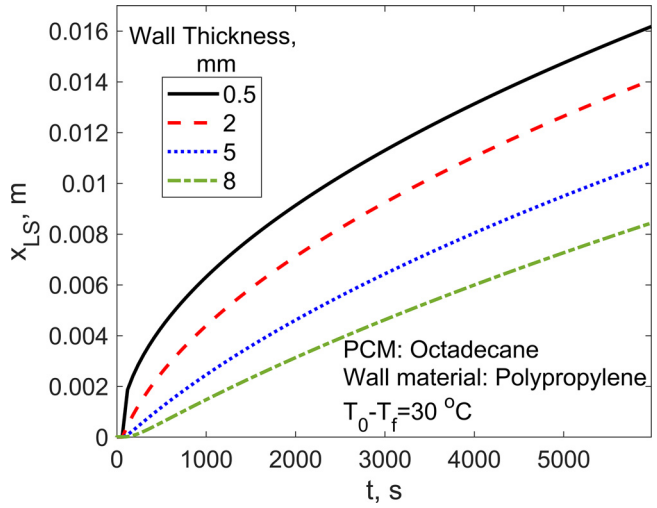

Fig. 15. Analysis of a practical problem: Phase change propagation front as a function of time for different thicknesses of a single-layered wall with octadecane phase change material and 30 K temperature boundary condition relative to melting temperature. Both wall and PCM are assumed to be at melting temperature initially. Plot is presented in dimensional form.

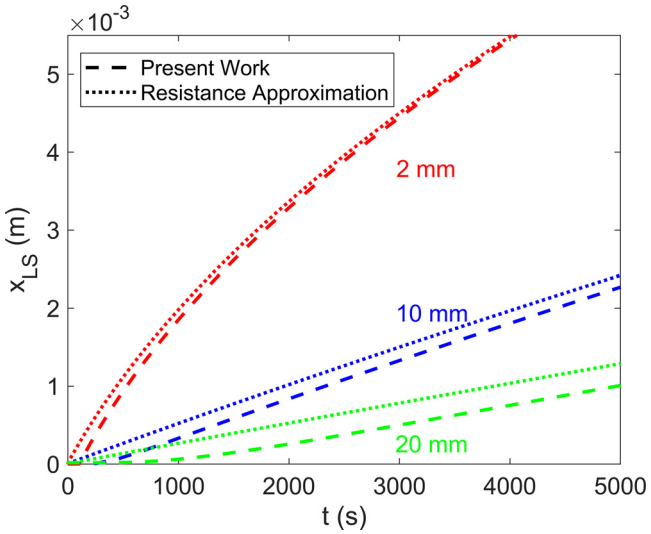

Fig. 16. Comparison of the present work with the convective resistance approximation: Phase change propagation as a function of time for a polypropylene wall for three different thicknesses. In each case, results from the present work and the convective resistance approximation are both plotted. The PCM is octadecane and a 10 K temperature rise in the wall is assumed.

mal diffusion through the wall. The thicker the wall, the longer is this initial period, before the phase change process accelerates. This initial period can be best seen for the 8 mm wall case shown in Fig. 15.

Plots such as ones presented in Figs. 14 and 15 provide useful design guidelines for practical latent heat energy storage systems containing a wall between the phase change material and the heat source/sink.

4.7. Comparison of the present work with a convective approximation

The present work accounts for the transient temperature distribution in the multilayer wall. In contrast, the presence of a wall may also be approximated by representing the wall as a thermal resistance, and therefore, modeling its effect in the form of a convective resistance at the boundary. While this represents some simplification in the problem, it still does not result in an analytical solution, since the Stefan problem with a convective heat transfer boundary does not have an analytical solution [42]. Moreover, the resistance approximation does not account for heat storage within the wall, which may be important at small times, particularly for thick, thermally insulating walls. In order to investigate this further, results from the present work are compared with numerical calculations based on the convective resistance approximation. Fig. 16 plots the phase change propagation front as a function of time for the melting of octadecane with a 10 °C temperature rise across a polypropylene wall of three different thicknesses. Results from the present work as well as the resistance approximation are plotted. Results for the resistance approximation are based on a variable timestep numerical calculation, since an analytical solution is not available. Fig. 16 shows that the resistance approximation is quite close to the present work when the wall is relatively thin. For thicker walls, however, the disagreement is larger, particularly at small times. The present work correctly accounts for heat storage in the wall, thereby predicting a flat phase change propagation curve at small times, whereas the resistance approximation incorrectly predicts very large rate of propagation at small times. The two curves tend to get closer to each other at large times when the effect of initial heat storage in the wall diminishes in comparison with latent heat storage in the PCM. Results from Fig. 16 show that the present work is particularly accurate for relatively thick, thermally insulating walls and for processes over relatively short time periods. For thin, conducting walls over long time periods, the resistance approximation is reasonably accurate because in such a case, energy storage in the wall is relatively less important.

5. Conclusions

The key results from this work include the derivation of a solution for phase change in the presence of a multi-layer wall between the PCM and heat source. This solution has been used to illustrate two key timescales present in the problem, as well as the impact of various non-dimensional parameters on the phase change process. Finally, this work also discusses practical problems related to design of a PCM wall for energy storage.

The solution technique uses the eigenfunction expansion method, which reduces the problem to that of thermal conduction through a multi-layer structure. Note that similar to most phase change heat transfer problems, the derived solution is not exact because at each time, it solves a transient problem that treats the melting front to be fixed at that time. While the solution technique used here is quite general, it is illustrated in this work for constant temperature source and for semi-infinite PCM that is initially at the melting temperature. The solution also applies to the case of a finite thickness PCM as long as the PCM is initially at the melting temperature, so that there is no heat transfer into the original phase. More complicated conditions, such as non-zero initial temperature of the PCM (Neumann problem) or a time-dependent temperature boundary condition can be easily modeled within the framework presented here. In the former case, an M+2 layer thermal conduction problem would need to be solved.

Finally, it is important to note other limitations of the present analysis, such as ignoring natural convection in the liquid, which may be reasonable for several scenarios, but may need to be accounted for in phase change problems with very large temperature difference, such as solidification of metals for casting and related manufacturing processes.

While presented in the context of melting, the results in this paper are equally applicable for solidification problems, as well as for equivalent mass transfer problems involving diffusion of species in conjunction with a chemical reaction front.

Declaration of Competing Interest

All authors hereby declare that they do not have conflicts of interest as described by Elsevier's policies (http://www.elsevier.com/conflictsofinterest).

CRediT authorship contribution statement

Mohammad Parhizi: Methodology, Formal analysis, Validation, Investigation, Data curation, Writing – original draft, Writing – review & editing. **Long Zhou:** Formal analysis, Investigation, Writing – original draft, Writing – review & editing. **Ankur Jain:** Conceptualization, Methodology, Formal analysis, Validation, Investigation, Data curation, Project administration, Writing – original draft, Writing – review & editing.

Data Availability

Data will be made available on request.

Acknowledgments

This material is based upon work supported by CAREER Award No. CBET-1554183 from the National Science Foundation. This paper is partly supported by the Key Scientific and Technological Breakthrough in Henan Province (No. 222102520007) and the Special Project of Basic Scientific Research Operating Expenses of Henan Polytechnic University (NSFRF210442).

Appendix A: Derivation of the eigenequation for general M-layered wall case

This Appendix derives the eigenequation for the general case of the M-layered wall. Section 2 shows that the general solution for $w_m(\xi,\tau)$ and $w_L(\xi,\tau)$ may be written as

$$w_m(\xi,\tau)=\sum_{n=1}^{\infty}c_n f_{m,n}(\xi)\exp\left(-\lambda_n^2\tau\right) \tag{A.1}$$

$$w_L(\xi,\tau)=\sum_{n=1}^{\infty}c_n f_{L,n}(\xi)\exp\left(-\lambda_n^2\tau\right) \tag{A.2}$$

where

$$f_{m,n}(\xi)=A_{m,n}\cos\left(\frac{\lambda_n}{\sqrt{\bar{\alpha}_m}}\xi\right)+B_{m,n}\sin\left(\frac{\lambda_n}{\sqrt{\bar{\alpha}_m}}\xi\right) \tag{A.3}$$

$$f_{L,n}(\xi)=A_{L,n}\cos\left(\frac{\lambda_n}{\sqrt{\bar{\alpha}_L}}\xi\right)+B_{L,n}\sin\left(\frac{\lambda_n}{\sqrt{\bar{\alpha}_L}}\xi\right) \tag{A.4}$$

One may re-write $f_{m,n}(\xi)$ as

$$f_{m,n}(\xi)=B_{1,n}\Phi_m p_{m,n}(\xi) \tag{A.5}$$

where $\Phi_1=1$ and

$$\Phi_m=\frac{p_{m-1,n}(\gamma_{m-1})-\bar{k}_{m-1}\bar{R}_{m-1}\dot{p}_{m-1,n}(\gamma_{m-1})}{p_{m,n}(\gamma_{m-1})}\cdot\frac{p_{m-2,n}(\gamma_{m-2})-\bar{k}_{m-2}\bar{R}_{m-2}\dot{p}_{m-2,n}(\gamma_{m-2})}{p_{m-1,n}(\gamma_{m-2})}\cdot\frac{p_{2,n}(\gamma_2)-\bar{k}_2\bar{R}_2\dot{p}_{2,n}(\gamma_2)}{p_{3,n}(\gamma_2)}\cdot\frac{p_{1,n}(\gamma_1)-\bar{k}_1\bar{R}_1\dot{p}_{1,n}(\gamma_1)}{p_{2,n}(\gamma_1)} \tag{A.6}$$

for m=2,3..M, and with

$$p_{m,n}(\xi)=\psi_{m,n}(\lambda_n)cos\left(\frac{\lambda_n}{\sqrt{\bar{\alpha}_m}}\xi\right)+sin\left(\frac{\lambda_n}{\sqrt{\bar{\alpha}_m}}\xi\right) \tag{A.7}$$

Note that the over-dot denotes the derivative with respect to ξ.

Further, the functions $\psi_{m,n}(\lambda_n)$ in Eq. (A.7) may be obtained from the boundary and interface conditions given by Eqs. (40)–(45) as follows:

$$\psi_{1,n}(\lambda_n)=0 \tag{A.8}$$

$$\psi_{m+1,n}(\lambda_n)=\frac{\bar{k}_{m+1}p_{m,n}(\gamma_m)\frac{\lambda_n}{\sqrt{\bar{\alpha}_{m+1}}}cos\left(\frac{\lambda_n\gamma_m}{\sqrt{\bar{\alpha}_{m+1}}}\right)-\bar{k}_m\dot{p}_{m,n}(\gamma_m)sin\left(\frac{\lambda_n\gamma_m}{\sqrt{\bar{\alpha}_{m+1}}}\right)-\bar{k}_m\bar{R}_m\dot{p}_{m,n}(\gamma_m)}{\bar{k}_{m+1}p_{m,n}(\gamma_m)\frac{\lambda_n}{\sqrt{\bar{\alpha}_{m+1}}}sin\left(\frac{\lambda_n\gamma_m}{\sqrt{\bar{\alpha}_{m+1}}}\right)+\bar{k}_m\dot{p}_{m,n}(\gamma_m)cos\left(\frac{\lambda_n\gamma_m}{\sqrt{\bar{\alpha}_{m+1}}}\right)}(m=1,2\ldots M-1) \tag{A.9}$$

$$\psi_{M,n}(\lambda_n)=-\frac{\tan\left(\frac{\lambda_n}{\sqrt{\bar{\alpha}_M}}\right)+\frac{\bar{k}_M}{\sqrt{\bar{\alpha}_M}}\tan\left(\lambda_n\xi_{LS}\right)-\frac{\lambda_n\bar{k}_M\bar{R}_M}{\sqrt{\bar{\alpha}_M}}}{1-\frac{\bar{k}_M}{\sqrt{\bar{\alpha}_M}}\tan\left(\lambda_n\xi_{LS}\right)\tan\left(\frac{\lambda_n}{\sqrt{\bar{\alpha}_M}}\right)+\frac{\lambda_n\bar{k}_M\bar{R}_M}{\sqrt{\bar{\alpha}_M}}\tan\left(\frac{\lambda_n}{\sqrt{\bar{\alpha}_M}}\right)} \tag{A.10}$$

The function $\psi_{M,n}(\lambda_n)$ for the M^{th} layer can be obtained from either Eq. (A.9) by setting m=M-1, or directly from Eq. (A.10). Therefore, the eigenvalues λ_n can be determined by comparing Eq. (A.10) with Eq. (A.9) for m=M-1. With some mathematical rearrangement, this results in

$$\frac{\bar{k}_M p_{M-1,n}(\gamma_{M-1})\frac{\lambda_n}{\sqrt{\bar{\alpha}_M}}\cos\left(\frac{\lambda_n\gamma_{M-1}}{\sqrt{\bar{\alpha}_M}}\right)-\bar{k}_{M-1}\dot{p}_{M-1,n}(\gamma_{M-1})\sin\left(\frac{\lambda_n\gamma_{M-1}}{\sqrt{\bar{\alpha}_M}}\right)-\bar{k}_{M-1}\bar{R}_{M-1}\dot{p}_{M-1,n}(\gamma_{M-1})}{\bar{k}_M p_{M-1,n}(\gamma_{M-1})\frac{\lambda_n}{\sqrt{\bar{\alpha}_M}}\sin\left(\frac{\lambda_n\gamma_{M-1}}{\sqrt{\bar{\alpha}_M}}\right)+\bar{k}_{M-1}\dot{p}_{M-1,n}(\gamma_{M-1})\cos\left(\frac{\lambda_n\gamma_{M-1}}{\sqrt{\bar{\alpha}_M}}\right)}$$
$$+\frac{\tan\left(\frac{\lambda_n}{\sqrt{\bar{\alpha}_M}}\right)+\frac{\bar{k}_M}{\sqrt{\bar{\alpha}_M}}\tan(\lambda_n\xi_{LS})-\frac{\bar{k}_M\bar{R}_M\lambda_n}{\sqrt{\bar{\alpha}_M}}}{1-\frac{\bar{k}_M}{\sqrt{\bar{\alpha}_M}}\tan(\lambda_n\xi_{LS})\tan\left(\frac{\lambda_n}{\sqrt{\bar{\alpha}_M}}\right)+\frac{\bar{k}_M\bar{R}_M\lambda_n}{\sqrt{\bar{\alpha}_M}}\tan\left(\frac{\lambda_n}{\sqrt{\bar{\alpha}_M}}\right)}=0 \tag{A.11}$$

which is the eigenequation for the general, M-layer case. The eigenequations λ_n for this problem can be obtained by determining the roots of Eq. (A.11).

Appendix B: Derivation of explicit recursive expressions for $A_{m,n}$, $B_{m,n}$, $A_{L,n}$ and $B_{L,n}$

This Appendix derives explicit recursive expressions for the coefficients $A_{m,n}$, $B_{m,n}$, $A_{L,n}$ and $B_{L,n}$ appearing in Eqs. (38) and (39) for the general, M-layered problem.

From Eq. (40), $A_{1,n}=0$. Further, due to the homogeneity and subsequent redundancy in the boundary and interface conditions given by Eqs. (40)–(45), one may choose, without loss of generality, one of the coefficients, $B_{1,n}$ in this case, to be one, while determining all other coefficients accordingly. Here, all remaining coefficients are determined in a recursive fashion, i.e., since $A_{1,n}$ and $B_{1,n}$ are known, therefore, $A_{m+1,n}$ and $B_{m+1,n}$ are determined in terms of $A_{m,n}$ and $B_{m,n}$ for m=1,2,3..M-1, and finally, $A_{L,n}$ and $B_{L,n}$ are determined in terms of $A_{M,n}$ and $B_{M,n}$. The following procedure is used:

From Eqs. (17) to (18), one may write, for each m=1,2,...M-1,

$$a_{m,n}A_{m+1,n}+b_{m,n}B_{m+1,n}=u_{m,n} \tag{B.1}$$

$$d_{m,n}A_{m+1,n}+e_{m,n}B_{m+1,n}=v_{m,n} \tag{B.2}$$

Where

$$a_{m,n}=\cos\left(\frac{\lambda_n\gamma_m}{\sqrt{\bar{\alpha}_{m+1}}}\right);\ b_{m,n}=\sin\left(\frac{\lambda_n\gamma_m}{\sqrt{\bar{\alpha}_{m+1}}}\right);\ d_{m,n}=-\frac{\bar{k}_{m+1}}{\sqrt{\bar{\alpha}_{m+1}}}\sin\left(\frac{\lambda_n\gamma_m}{\sqrt{\bar{\alpha}_{m+1}}}\right);\ e_{m,n}=\frac{\bar{k}_{m+1}}{\sqrt{\bar{\alpha}_{m+1}}}\cos\left(\frac{\lambda_n\gamma_m}{\sqrt{\bar{\alpha}_{m+1}}}\right) \tag{B.3}$$

$$u_{m,n}=A_{m,n}\left[\cos\left(\frac{\lambda_n\gamma_m}{\sqrt{\bar{\alpha}_m}}\right)-\bar{k}_m\bar{R}_m\frac{\lambda_n}{\sqrt{\bar{\alpha}_m}}\sin\left(\frac{\lambda_n\gamma_m}{\sqrt{\bar{\alpha}_m}}\right)\right]+B_{m,n}\left[\sin\left(\frac{\lambda_n\gamma_m}{\sqrt{\bar{\alpha}_m}}\right)+\bar{k}_m\bar{R}_m\frac{\lambda_n}{\sqrt{\bar{\alpha}_m}}\cos\left(\frac{\lambda_n\gamma_m}{\sqrt{\bar{\alpha}_m}}\right)\right] \tag{B.4}$$

$$v_{m,n}=\frac{\bar{k}_m}{\sqrt{\bar{\alpha}_m}}\left[-A_{m,n}\sin\left(\frac{\lambda_n\gamma_m}{\sqrt{\bar{\alpha}_m}}\right)+B_{m,n}\cos\left(\frac{\lambda_n\gamma_m}{\sqrt{\bar{\alpha}_m}}\right)\right] \tag{B.5}$$

Eqs. (B.1) and (B.2) represent a set of two linear equations in $A_{m+1,n}$ and $B_{m+1,n}$. A solution is given by

$$A_{m+1,n}=\frac{e_{m,n}u_{m,n}-b_{m,n}v_{m,n}}{a_{m,n}e_{m,n}-b_{m,n}d_{m,n}};\ B_{m+1,n}=\frac{-d_{m,n}u_{m,n}+a_{m,n}v_{m,n}}{a_{m,n}e_{m,n}-b_{m,n}d_{m,n}} \tag{B.6}$$

Note that $u_{m,n}$ and $v_{m,n}$ are known in terms of $A_{m,n}$ and $B_{m,n}$. Therefore, Eq. (B.6) recursively expresses $A_{m+1,n}$ and $B_{m+1,n}$ in terms of $A_{m,n}$ and $B_{m,n}$ for m=1,2..M-1. Finally, $A_{L,n}$ and $B_{L,n}$ can be expressed in terms of $A_{M,n}$ and $B_{M,n}$ using a similar procedure. From Eqs. (43) to (44),

$$a_{M,n}A_{L,n}+b_{M,n}B_{L,n}=u_{M,n} \tag{B.7}$$

$$d_{M,n}A_{L,n}+e_{M,n}B_{L,n}=v_{M,n} \tag{B.8}$$

where

$$a_{M,n}=\cos(\lambda_n);\ b_{m,n}=\sin(\lambda_n);\ d_{m,n}=-\sin(\lambda_n);\ e_{m,n}=\cos(\lambda_n) \tag{B.9}$$

$$u_{m,n}=A_{M,n}\left[\cos\left(\frac{\lambda_n}{\sqrt{\bar{\alpha}_M}}\right)+\bar{k}_M\bar{R}_M\frac{\lambda_n}{\sqrt{\bar{\alpha}_M}}\sin\left(\frac{\lambda_n}{\sqrt{\bar{\alpha}_M}}\right)\right]+B_{M,n}\left[\sin\left(\frac{\lambda_n}{\sqrt{\bar{\alpha}_M}}\right)-\bar{k}_M\bar{R}_M\frac{\lambda_n}{\sqrt{\bar{\alpha}_M}}\cos\left(\frac{\lambda_n}{\sqrt{\bar{\alpha}_M}}\right)\right] \tag{B.10}$$

$$v_{m,n}=\frac{\bar{k}_M}{\sqrt{\bar{\alpha}_M}}\left[-A_{M,n}\sin\left(\frac{\lambda_n}{\sqrt{\bar{\alpha}_M}}\right)+B_{M,n}\cos\left(\frac{\lambda_n}{\sqrt{\bar{\alpha}_M}}\right)\right] \tag{B.11}$$

Therefore, $A_{L,n}$ and $B_{L,n}$ are given by

$$A_{L,n}=\frac{e_{M,n}u_{M,n}-b_{M,n}v_{M,n}}{a_{M,n}e_{M,n}-b_{M,n}d_{M,n}};\ B_{L,n}=\frac{-d_{M,n}u_{M,n}+a_{M,n}v_{M,n}}{a_{M,n}e_{M,n}-b_{M,n}d_{M,n}} \tag{B.12}$$

References

[1] B. Liu, P. Majumdar, Numerical simulation of phase change heat transfer in PCM encapsulated heat sinks, in: Proceedings of the 10th Intersociety Conference on Thermal and Thermomechanical Phenomena in Electronics Systems, 2006, doi:10.1109/ITHERM.2006.1645363.

[2] A. Mostafavi, M. Parhizi, A. Jain, Semi-analytical thermal modeling of transverse and longitudinal fins in a cylindrical phase change energy storage system, Int. J. Therm. Sci. 153 (2020) 106352, doi:10.1016/j.ijthermalsci.2020.106352.

[3] P. Foteinopoulos, A. Papacharalampopoulos, P. Stavropoulos, On thermal modeling of additive manufacturing processes, CIRP J. Manuf. Sci. Technol. 20 (2018) 66–83, doi:10.1016/j.cirpj.2017.09.007.

[4] J.A.D. Mannapperuma, R.P. Singh, Prediction of freezing and thawing times of foods using a numerical method based on enthalpy formulation, J. Food Sci. 53 (2) (1988) 626–630, doi:10.1111/j.1365-2621.1988.tb07770.x.

[5] R. Viskanta, Heat transfer during melting and solidification of metals, J. Heat Transf. 110 (1988) 1205–1291, doi:10.1115/1.3250621.

[6] V. Alexiades, A.D. Solomon, Mathematical Modeling of Melting and Freezing Processes, CRC Press, 1993.

[7] V.J. Lunardini, Heat Transfer With Freezing and Thawing, Elsevier, 1991.

[8] A. Mori, K. Araki, Methods for analysis of moving boundary-surface problem, Int. Chem. Eng. 16 (4) (1976) 734–744.

[9] D.A. Tarzia, "A bibliography on moving-free boundary problems for the heat-diffusion equation," Stefan and related problems, MAT-Serie A, vol. 2, 2000.

[10] D.W. Hahn, M.N. Özişik, Heat Conduction, Wiley, 2012 ISBN: 978-0-470-90293-6.

[11] D. Mazzeo, G. Oliveti, M. De Simone, N. Arcuri, Analytical model for solidification and melting in a finite PCM in steady periodic regime, Int. J. Heat Mass Transf. 88 (2015) 844–861, doi:10.1016/j.ijheatmasstransfer.2015.04.109.

[12] T.R. Goodman, The heat balance integral methods and its application to problems involving a change of phase, Trans. ASME 80 (1958) 335–342.

[13] M. Parhizi, A. Jain, Solution of the phase change Stefan problem with time-dependent heat flux using perturbation method, J. Heat Transf. 141 (2019) 024503: 1-5, doi:10.1115/1.4041956.

[14] M. Ozisik, S. Guçeri, A variable eigenvalue approach to the solution of phase-change problems, Can. J. Chem. Eng. 55 (2) (1977) 145–148, doi:10.1002/cjce.5450550207.

[15] S. Svetislav, J. Caldwell, Numerical solution of Stefan problem with time-dependent boundary conditions by variable space grid method, Therm. Sci. 13 (2009) 165–175, doi:10.2298/TSCI0904165S.

[16] M.F. Natale, D.A. Tarzia, Explicit solutions to the one-phase Stefan problem with temperature-dependent thermal conductivity and a convective term, Int. J. Eng. Sci. 41 (15) (2003) 1685–1698, doi:10.1016/S0020-7225(03)00067-3.

[17] A.K. Singh, A. Kumar, Rajeev, A Stefan problem with variable thermal coefficients and moving phase change material, J. King Saud Univ. Sci. 31 (2019) 1064–1069, doi:10.1016/j.jksus.2018.09.009.

[18] A. Jain, M. Parhizi, Conditionally exact closed-form solution for moving boundary problems in heat and mass transfer in the presence of advection, Int. J. Heat Mass Transf. 180 (2021) 121802, doi:10.1016/j.ijheatmasstransfer.2021.121802.

[19] H. Hu, S.A. Argyropoulos, Mathematical modelling of solidification and melting: a review, Modell. Simul. Mater. Sci. Eng. 4 (1996) 371–396, doi:10.1088/0965-0393/4/4/004.

[20] D. Mazzeo, G. Oliveti, Parametric study and approximation of the exact analytical solution of the Stefan problem in a finite PCM layer in a steady periodic regime, Int. Commun. Heat Mass Transf. 84 (2017) 49–65, doi:10.1016/j.icheatmasstransfer.2017.03.013.

[21] D. Mazzeo, G. Oliveti, Thermal field and heat storage in a cyclic phase change process caused by several moving melting and solidification interfaces in the layer, Int. J. Therm. Sci. 129 (2018) 462–488, doi:10.1016/j.ijthermalsci.2017.12.026.

[22] N. Gol'dman, Inverse Stefan Problems, 1st ed., Springer, 1997. ISBN: 978-94-011-5488-8.

[23] J. Crank, Two methods for the numerical solution of moving-boundary problems in diffusion and heat flow, Q. J. Mech. Appl. Math. 10 (2) (1957) 220–231, doi:10.1093/qjmam/10.2.220.

[24] R. Furzeland, A comparative study of numerical methods for moving boundary problems, IMA J. Appl. Math. 26 (4) (1980) 411–429, doi:10.1093/imamat/26.4.411.

[25] V. Voller, M. Cross, Accurate solutions of moving boundary problems using the enthalpy method, Int. J. Heat Mass Transf. 24 (3) (1981) 545–556, doi:10.1016/0017-9310(81)90062-4.

[26] A. Caggiano, C. Mankel, E. Koenders, Reviewing theoretical and numerical models for PCM-embedded cementitious composites, Buildings 9 (2019) 1–26, doi:10.3390/buildings9010003.

[27] H. Wang, C. An, M. Duan, J. Su, Transient thermal analysis of multilayer pipeline with phase change material, Appl. Therm. Eng. 165 (2020) 114512 1-13, doi:10.1016/j.applthermaleng.2019.114512.

[28] P.A. Mirzai, F. Haghighat, Modeling of phase change materials for applications in whole building simulation, Renew. Sustain. Energy Rev. 16 (2012) 5355–5362, doi:10.1016/j.rser.2012.04.053.

[29] N. Zhu, P. Hu, L. Xu, A simplified dynamic model of double layers shape-stabilized phase change materials wallboards, Energy Build. 67 (2013) 508–516, doi:10.1016/j.enbuild.2013.08.043.

[30] A.A. Al-Abidi, S. Mat, K. Sopian, M.Y. Sulaiman, A. Mohammad, Numerical study of PCM solidification in a triplex tube heat exchanger with internal and external fins, Int. J. Heat Mass Transf. 61 (2013) 684–695, doi:10.1016/j.ijheatmasstransfer.2013.02.030.

[31] M. Izquierdo-Barrientos, J.F. Belmonte, D. Rodríguez-Sánchez, A.E. Molina, J.A. Almendros-Ibáñez, A numerical study of external building walls containing phase change materials (PCM), Appl. Therm. Eng. 47 (2012) 73–85, doi:10.1016/j.applthermaleng.2012.02.038.

[32] F. Mathieu-Potvin, L. Gosselin, Thermal shielding of multilayer walls with phase change materials under different transient boundary conditions, Int. J. Therm. Sci. 48 (2009) 1707–1717, doi:10.1016/j.ijthermalsci.2009.01.010.

[33] M. Amara, V. Timchenko, M. El Ganaoui, E. Leonardi, G. Davis, A 3D computational model of heat transfer coupled to phase change in multilayer materials with random thermal contact resistance, Int. J. Therm. Sci. 48 (2009) 421–427, doi:10.1016/j.ijthermalsci.2008.03.008.

[34] C.-C. Hwang, S. Lin, L.-F. Shen, Effects of wall conduction and interface thermal resistance on the phase-change problem, Int. J. Heat Mass Transf. 37 (1994) 1849–1855, doi:10.1016/S0017-9310(99)00178-7.

[35] H. Qarnia, F. Adnani, E. Lakhal, Approximate analytical solution for one-dimensional solidification problem of a finite superheating phase change material including the effects of wall and thermal contact resistances, J. Appl. Math. (2012) 174604 1-21, doi:10.1155/2012/174604.

[36] M. Parhizi, A. Jain, Theoretical modeling of a phase change heat transfer problem with a pre-melted or pre-solidified region, Int. J. Heat Mass Transf. 136 (2019) 635–643, doi:10.1016/j.ijheatmasstransfer.2019.02.079.

[37] M.D. Mikhailov, M.N. Özişik, Unified Analysis and Solutions of Heat and Mass Diffusion, Dover Publications, New York, 1994.

[38] B.F. Blackwell, W. Gill, K. Dowding, T. Voth, Determination of thermal conductivity of 304 stainless steel using parameter estimation techniques, in: Proceedings of the 34th National Heat Transfer Conference, Pittsburgh, PA, 2000.

[39] www.professionalplastics.com, last accessed Aug 6, 2021.

[40] N.R. Jankowski, F.P. McCluskey, A review of phase change materials for vehicle component thermal buffering, Appl. Energy 113 (2014) 1525–1561, doi:10.1016/j.apenergy.2013.08.026.

[41] A. Mostafavi, M. Parhizi, A. Jain, Theoretical modeling and optimization of fin-based enhancement of heat transfer into a phase change material, Int. J. Heat Mass Transf. 145 (2019) 118698 1-10, doi:10.1016/j.ijheatmasstransfer.2019.118698.

[42] D.A. Tarzia, 'An explicit solution for a two-phase unidimensional Stefan problem with a convective boundary condition at the fixed face,' MAT - Serie A, 8, pp. 21-27, 2004.